

# DVD: Deterministic Video Depth Estimation with Generative Priors

Hongfei Zhang<sup>1†</sup>, Harold Haodong Chen<sup>1,2†</sup>, Chenfei Liao<sup>1†</sup>, Jing He<sup>1†</sup>, Zixin Zhang<sup>1</sup>, Haodong Li<sup>3</sup>, Yihao Liang<sup>4</sup>, Kanghao Chen<sup>1</sup>, Bin Ren<sup>5</sup>, Xu Zheng<sup>1</sup>, Shuai Yang<sup>1</sup>, Kun Zhou<sup>6</sup>, Yinchuan Li<sup>7</sup>, Nicu Sebe<sup>8</sup>, Ying-Cong Chen<sup>1,2‡</sup>

<sup>1</sup>HKUST(GZ), <sup>2</sup>HKUST, <sup>3</sup>UCSD, <sup>4</sup>Princeton University, <sup>5</sup>MBZUAI, <sup>6</sup>SZU, <sup>7</sup>Knowin, <sup>8</sup>UniTrento  
<sup>†</sup>Equal Contribution, <sup>‡</sup>Corresponding Author

Existing video depth estimation faces a fundamental trade-off: *generative models* suffer from stochastic geometric hallucinations and scale drift, while *discriminative models* demand massive labeled datasets to resolve semantic ambiguities. To break this impasse, we present **DVD**, the *first* framework to deterministically adapt pre-trained video diffusion models into single-pass depth regressors. Specifically, **DVD** features three core designs: (i) repurposing the diffusion **timestep as a structural anchor** to balance global stability with high-frequency details; (ii) **latent manifold rectification (LMR)** to mitigate regression-induced over-smoothing, enforcing differential constraints to restore sharp boundaries and coherent motion; and (iii) **global affine coherence**, an inherent property bounding inter-window divergence, which enables seamless long-video inference without requiring complex temporal alignment. Extensive experiments demonstrate that **DVD** achieves *state-of-the-art* zero-shot performance across benchmarks. Furthermore, **DVD** successfully unlocks the profound geometric priors implicit in video foundation models using  $163\times$  *less* task-specific data than leading baselines. Notably, we fully release our pipeline, providing the *whole training suite* for SOTA video depth estimation to benefit the open-source community.

📅 **Date:** March 13, 2026

🌐 **Project:** <https://dvd-project.github.io/>

👉 **Github:** <https://github.com/EnVision-Research/DVD>

## 1 Introduction

Depth estimation serves as a fundamental building block for 3D scene understanding, underpinning applications (Chen et al., 2025e; Charatan et al., 2024; Xu et al., 2025a; Zhang et al., 2023; O’Neill et al., 2024) from autonomous driving to robotic manipulation. While image-based depth estimation has matured significantly (Bochkovskii et al., 2024; Yang et al., 2024c,b; Piccinelli et al., 2024; Yin et al., 2023; Fu et al., 2024), elevating this capability to the video domain remains a formidable challenge. The transition from static images to dynamic video is non-trivial; it demands not only precise geometric reasoning per frame but also rigorous temporal consistency. In real-world scenarios characterized by camera motion and dynamic objects, maintaining this consistency without sacrificing high-frequency geometric details is a persistent bottleneck.

Recent advances in video depth estimation have predominantly followed two paradigms, each constrained by inherent limitations that hinder their broader applicability, as shown in Figure 1 (*Top*). (I) **Diffusion-based generative models** (Hu et al., 2025; Shao et al., 2025; Yang et al., 2024a) (*e.g.*, DepthCrafter) leverage pre-trained video foundation models to capture rich spatio-temporal priors, enabling impressive zero-shot generalization. However, their reliance on stochastic sampling introduces temporal uncertainties which limit their stability and reliability in real-world applications. Moreover, the generative nature of these models tends to prioritize visual plausibility over geometric accuracy, leading to **geometric hallucination**, a failure to maintain precise and globally consistent geometry over time. (II) **Discriminative ViT-based models** (Yang et al., 2024c; Chen et al., 2025d) (*e.g.*, Video Depth Anything, VDA), on the other hand, provide high inference efficiency and deterministic outputs. Yet, learning geometry strictly from dense annotations, they frequently suffer from **semantic ambiguity**, misinterpreting motion blur or textureless regions as structural boundaries. To

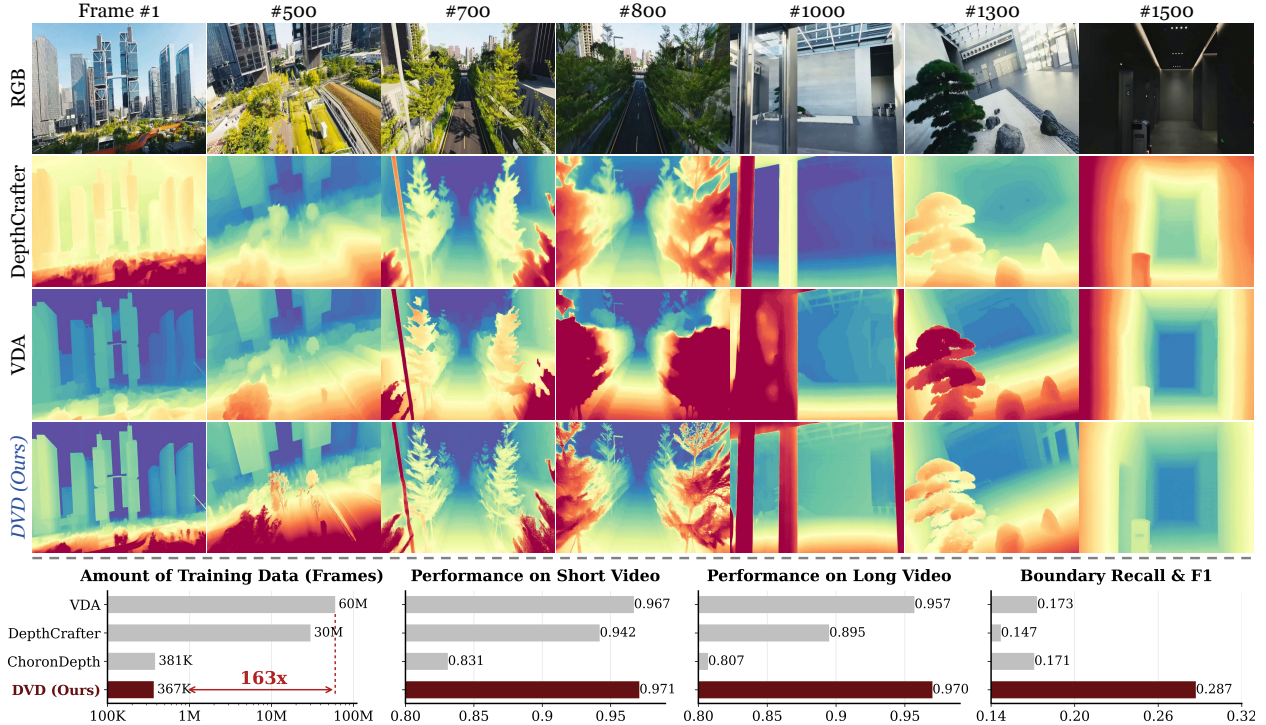


**Figure 1 (Top)** Comparisons on a 1500-frame in-the-wild video highlight a fundamental paradigm trade-off: representative generative models (*e.g.*, DepthCrafter (Hu et al., 2025)) suffer from *geometric hallucination*, while leading discriminative baselines (*e.g.*, VDA (Chen et al., 2025d)) face *semantic ambiguity*. **DVD** resolves this dilemma, delivering consistent, high-fidelity geometry. **(Bottom)** **DVD** achieves superior performance on both short and long videos (averaged on KITTI (Geiger et al., 2012), ScanNet (Dai et al., 2017), and Bonn (Palazzolo et al., 2019)), while successfully unlocking the rich priors implicit in video foundation models using remarkably minimal task-specific data, *e.g.*, less than 1% of VDA’s training set.

overcome this ambiguity, discriminative paradigms heavily rely on massive-scale and diversified downstream annotations (Chen et al., 2025d; Yang et al., 2024b,c; Birkel et al., 2023). This extreme data dependency not only raises significant barriers to scalability and reproducibility but also restricts their adaptability in broader, data-scarce scenarios. These aforementioned challenges lead to our pivotal research question:

🔍 *Can we design a video depth estimation framework that effectively balances the structural stability of discriminative models and the rich spatio-temporal priors of generative approaches, while remaining efficient and scalable?*

In response, we present **DVD**, a novel framework that achieves deterministic video depth estimation with generative priors. Departing from the conventional stochastic generative paradigm, **DVD** pioneers the deterministic adaptation of pre-trained video diffusion models, learning a direct mapping from RGB latents to depth latents. This paradigm shift introduces a new design point: leveraging the backbone’s rich semantic priors to resolve motion-induced ambiguity while enforcing a regression objective that predicts geometrically consistent depth, effectively mitigating generative hallucination. However, extending deterministic adaptation from static images (Lee et al., 2024; He et al., 2025) to dynamic videos, presents unique challenges: a naive regression is not merely prone to *blurring*, but suffers from *structural instability* and *scalability* issues (Hu et al., 2025; Shao et al., 2025).

To address these bottlenecks, **DVD** introduces a video deterministic adaptation paradigm built upon three key mechanisms: **1 Timestep as a Structural Anchor**: We repurpose the diffusion timestep  $t$  from a noise-level index into a structural anchor, effectively balancing low-frequency geometric stability with high-frequency spatial details. **2 Latent Manifold Rectification (LMR)**: To combat the fundamental spatio-temporal "mean collapse" in deterministic regression, we introduce a parameter-free supervision that aligns latent differentials, successfully restoring sharp boundaries and coherent motion. **3 Global Affine Coherence**: We uncover that our deterministic

backbone inherently bounds inter-window divergence. This property enables a seamless, affine-alignment sliding-window inference strategy for long-duration videos, bypassing complex latent stitching (Hu et al., 2025; Shao et al., 2025). Ultimately, **DVD** resolves the ambiguity-hallucination dilemma by successfully repurposing video generation models into deterministic regressors. This paradigm shift achieves *state-of-the-art* zero-shot video depth estimation. Notably, **DVD** effectively unlocks the rich geometric priors embedded in foundation models using remarkably minimal task-specific data. This establishes a highly efficient and scalable adaptation route for future 3D perception. In brief, our contributions are summarized as follows:

- **Bottleneck Identification.** Through analysis of existing video depth estimation paradigms, we identify key bottlenecks: geometric hallucination in generative models and semantic ambiguity in discriminative models, which hinder scalability and practical deployment.
- **Our Solution.** We present **DVD**, which pioneers the deterministic adaptation of pre-trained video diffusion models into single-pass regressors. **DVD** leverages three key insights to address the identified bottlenecks: (i) timestep as a structural anchor, which balances the trade-off between geometric stability and detail precision; (ii) latent manifold rectification, which ensures spatial and temporal consistency; and (iii) global affine coherence, which enables robust long-video inference.
- **Empirical Validation.** Extensive experiments across four real-world benchmarks demonstrate that **DVD** achieves ① **superior performance:** achieving *state-of-the-art* zero-shot geometric fidelity and temporal coherence; ② **compelling efficiency:** successfully unlocking pre-trained world priors with remarkably minimal downstream data (*e.g.*, < 1% of leading baselines) while maintaining comparable inference speed; and ③ **robust scalability:** enabling seamless, robust inference on long videos and effortlessly generalizing to unconstrained open-world domains.

## 2 Related Work

**Monocular Depth Estimation.** Modern approaches have evolved from handcrafted features to data-driven deep learning (Bhat et al., 2021; Eigen et al., 2014), broadly categorizing into two dominant paradigms: **(I) Discriminative Regression:** This paradigm leverages ViTs and large-scale supervision to learn direct depth mappings (Chou et al., 2025; Hu et al., 2024; Wang et al., 2025; Birkl et al., 2023; Sobko et al., 2026; Piccinelli et al., 2025). Foundation models like Depth Anything V1/V2 (Yang et al., 2024b,c; Pham et al., 2025) demonstrate robust zero-shot generalization by scaling up unlabeled pre-training. To recover metric scale, approaches such as Metric3D (Yin et al., 2023), UniDepth (Piccinelli et al., 2024), and Depth Pro (Bochkovskii et al., 2024) focus on resolving focal length ambiguities and preserving high-frequency details. In the video domain, methods like Video Depth Anything (Chen et al., 2025d) extend these backbones with temporal modules or flow-based refinement. While efficient and deterministic, discriminative methods typically lack the generative priors necessary to resolve semantic ambiguities in textureless or motion-blurred regions. **(II) Generative Diffusion:** To incorporate rich geometric priors, recent works repurpose pre-trained diffusion models for depth estimation (Song et al., 2025; Kong et al., 2025; Li et al., 2025; Ranftl et al., 2021; Bhat et al., 2023; Yang et al., 2024a). Image-based methods, such as Marigold (Ke et al., 2025c) and Lotus (He et al., 2024, 2025), fine-tune latent diffusion models to achieve superior structural detail compared to discriminative baselines. Video-specific approaches, including ChronoDepth (Shao et al., 2025), DepthCrafter (Hu et al., 2025), and RollingDepth (Ke et al., 2025b), further adapt these priors to model temporal dynamics. However, their reliance on stochastic multi-step sampling inherently introduces high latency and geometric hallucinations, a bottleneck our **DVD** resolves via deterministic adaptation.

**Video Diffusion Models.** The field has witnessed a paradigm shift from adapting 2D U-Nets (Ronneberger et al., 2015) to scalable diffusion transformers (DiT) (Peebles and Xie, 2023). Early pioneering works (Blattmann et al., 2023a,b; Ho et al., 2022; Guo et al., 2023; Wang et al., 2023) primarily extended pre-trained image architectures by inserting temporal attention or 3D convolutions. Recently, a paradigm shift has occurred driven by spacetime patchified sequence modeling (Brooks et al., 2024) and continuous flow matching (Lipman et al., 2022). By scaling DiT with advanced 3D VAEs, modern foundation models (Team, 2024; Seedance et al., 2025; Gao et al., 2025; Chen et al., 2025a), such as CogVideoX (Hong et al., 2022; Chen et al., 2025b; Chen et al.), HunyuanVideo (Kong et al., 2024), and Wan (Wan et al., 2025; Zhang et al., 2025), have demonstrated

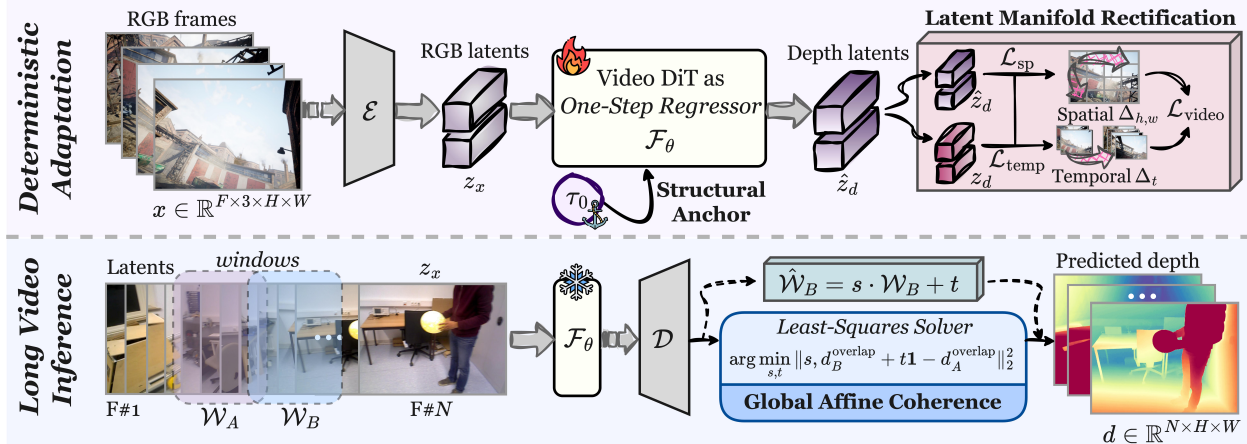


**Figure 2 Overview of DVD.** (Top) A video DiT ( $\mathcal{F}_\theta$ ) performs single-pass depth regression, modulated by a structural anchor ( $\tau_0$ ). Latent manifold rectification (LMR) mitigates mean collapse via differential constraints. (Bottom) For long video depth estimation, overlapping windows ( $\mathcal{W}_A, \mathcal{W}_B$ ) are seamlessly aligned using a closed-form least-squares solver, leveraging the model’s global affine coherence.

unprecedented capabilities in simulating physical dynamics and maintaining strict 3D consistency (Huang et al., 2024; Chen et al., 2025c). These foundation models effectively function as world simulators, encoding rich geometric and dynamic priors that **DVD** repurposes for deterministic depth regression.

**More Video Depth Methods.** Beyond the generative and discriminative paradigms for relative video depth discussed above, recent advancements have diversified video depth estimation into several specialized tracks. One prominent direction optimizes for (I) **real-time streaming efficiency**, with methods like FlashDepth (Chou et al., 2025) and VeloDepth (Piccinelli et al., 2025) employing lightweight architectures for latency-critical applications. Other parallel tracks like (II) **metric geometry recovery**, where GeometryCrafter (Xu et al., 2025b) alters the target representation to unbounded point maps to facilitate downstream 3D/4D reconstruction. While these works make significant strides in their respective settings, their primary objectives diverge fundamentally from our problem formulation, where **DVD** explores a more general direction for video depth. Consequently, these works also serve as valuable complementary approaches to the field, rather than direct baselines for our core setting.

## 3 Preliminary

### 3.1 Problem Formulation

We formalize video depth estimation as a mapping from an input RGB sequence  $x \in \mathbb{R}^{F \times 3 \times H \times W}$  to its corresponding depth sequence  $d \in \mathbb{R}^{F \times H \times W}$ , where  $F$  denotes the frame count. To exploit the rich semantic priors of large-scale pre-trained models, we operate within a compressed latent manifold. Specifically, a frozen variational autoencoder (VAE) encoder  $\mathcal{E}(\cdot)$  projects both RGB and depth into a unified latent space:

$$z_x = \mathcal{E}(x) \in \mathbb{R}^{f \times C \times h \times w}, \quad z_d = \mathcal{E}(d) \in \mathbb{R}^{f \times C \times h \times w}, \quad (1)$$

where  $c, f, h, w$  represent the latent channels and downsampled dimensions, respectively. Our objective is to learn a deterministic mapping  $\Phi: z_x \mapsto z_d$  that recovers the geometric structure directly in the latent space. The final depth  $\hat{d}$  is reconstructed via the frozen VAE decoder  $\hat{d} = \mathcal{D}(\hat{z}_d)$ .

### 3.2 Diffusion as Deterministic Regressor

**Role of  $t$  in Rectified Flow.** In traditional rectified flow (RF) (Liu et al., 2022; Lipman et al., 2022), the time variable  $t \in [0, 1]$  explicitly parameterizes a noise interpolation trajectory between data distribution  $z_0 \sim p_{\text{data}}$  and Gaussian noise  $z_1 \sim \mathcal{N}(0, I)$ . RF defines a linear interpolation trajectory  $z_t = (1-t)z_0 + tz_1$ , where the scalar timestep  $t \in [0, 1]$  explicitly parameterizes the corruption level. The network  $v_\theta$  is trained to predict

the velocity field of this flow by minimizing:

$$\mathcal{L}_{\text{RF}} = \mathbb{E}[\|v_{\theta}(z_t, t) - (z_1 - z_0)\|^2]. \quad (2)$$

During standard generative inference, one produces samples by solving the ordinary differential equation (ODE)  $dz_t/dt = v_{\theta}(z_t, t)$  via numerical integration from  $t = 1$  to  $t = 0$ .

**Deterministic Adaptation.** Recent works in the image domain (He et al., 2024, 2025) repurpose diffusion backbones as *one-step deterministic regressors*. Instead of iterative ODE integration over a noise trajectory, the network  $\mathcal{F}_{\theta}$  performs a direct functional mapping. Formally, given the RGB latent  $z_x$  and a timestep condition  $t$ , depth is deterministically predicted in a single forward pass:

$$\hat{z}_d = \mathcal{F}_{\theta}(z_x, t). \quad (3)$$

Building upon this static-image formulation, Section §4 details how **DVD** extends this paradigm to videos, along with uncovering a crucial functional shift for the timestep  $t$  to preserve geometric consistency.

## 4 Methodology

### 4.1 Overall Framework

Existing video depth estimation methods are typically polarized: generative diffusion models offer rich spatio-temporal priors but suffer from stochastic geometric hallucinations, while discriminative regressors provide stable outputs but demand massive labeled datasets to resolve semantic ambiguities. Our **DVD** is proposed to bridge this gap, a novel framework that unites the generalization power of generative priors with the structural stability of deterministic regression, as shown in Figure 2. Formally, given an input RGB video  $x$ , a VAE encoder  $\mathcal{E}$  extracts the latent representation  $z_x$ . This latent sequence is then processed by a pre-trained video diffusion backbone  $\mathcal{F}_{\theta}$ . Instead of performing iterative stochastic denoising, **DVD** executes a single-pass deterministic mapping to predict the depth latent  $\hat{z}_d$ , modulated by a conditioning timestep  $\tau$ :

$$\hat{z}_d = \mathcal{F}_{\theta}(z_x, \tau(t)). \quad (4)$$

To achieve high-fidelity depth estimation, **DVD** introduces three core designs tailored to the latent dynamics of video diffusion backbones. First, we repurpose the diffusion timestep  $\tau$  as a *structural anchor* (Section §4.2) to govern the backbone’s geometric operating regime, balancing low-frequency stability with high-frequency details. Then, we introduce *latent manifold rectification* (Section §4.3), a parameter-free supervision mechanism that enforces differential consistency to mitigate regression-induced mean collapse and sharpen spatio-temporal boundaries. Finally, we present *global affine coherence* (Section §4.4), an inherent property of our deterministic backbone that strictly bounds inter-window divergence, enabling seamless, affine-alignment inference for long-duration videos. We next detail the empirical observations and technical formulations that motivate these designs in the following sections.

### 4.2 Timestep as Structural Anchor

In single-image deterministic adaptation (*e.g.*, Lotus (He et al., 2024, 2025)), the diffusion timestep is typically fixed at the terminal state ( $t = 1$ ) or absorbed entirely. However, we empirically observe that applying this to video backbones causes severe geometric over-smoothing (Figure 3). We attribute this to the spectral bias inherent in the pre-trained diffusion priors (Kingma et al., 2021; Choi et al., 2022; Hang et al., 2025, 2023; Ho et al., 2022). During generative pre-training, the timestep  $t$  parameterizes the signal-to-noise ratio (SNR): a higher  $t$  (early time, low SNR) forces the network to estimate low-frequency global structures, while a lower  $t$  (late time, high SNR) trains the network to resolve high-frequency local details. Therefore, in our deterministic adaptation, the timestep transcends its traditional role as a noise indicator. By replacing the dynamic timestep  $t$  with a conditioning state  $\tau_0$ , we instantiate a persistent **structural anchor** that explicitly modulates the network’s geometric operating regime.

**Frequency-Parameterized Conditioning.** To better understand this mechanism, we analyze how  $t$  enters the network. In **DVD**,  $t$  acts as a frequency-parameterized condition via a fixed sinusoidal basis (Kim et al., 2024; Wan et al., 2025):

$$\mathbf{e}_{\text{sin}}(t) = [\cos(\omega_1 t), \dots, \cos(\omega_{d/2} t), \sin(\omega_1 t), \dots, \sin(\omega_{d/2} t)], \quad (5)$$

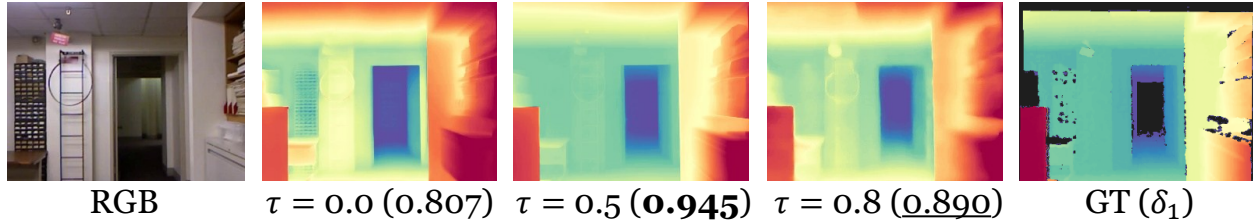


**Figure 3 Timestep as a structural anchor.** Visualizations on NYU (Nathan Silberman and Fergus, 2012) demonstrate a fidelity-stability trade-off. Low ( $\tau = 0.0$ ) recovers sharp boundaries but lacks global consistency, whereas high ( $\tau = 0.8$ ) causes detail loss (e.g., blur). An optimal anchor ( $\tau = 0.5$ ) balances these regimes, achieving a trade-off between detail recovery and metric accuracy. More detailed quantitative analyses are shown in Figure 10.

where  $d$  is the embedding dimension and  $\{\omega_i\}$  are predefined angular frequencies. Rather than sampling  $t \sim \mathcal{U}(0, 1)$ , **DVD** anchors the model to a single optimal state  $\tau_0$ . This instantiates a persistent structural code that calibrates the backbone’s conditioning pathway. The deterministic mapping is thus formulated as:

$$\hat{z}_d = \mathcal{F}_\theta(z_x; \mathbf{e}_\phi(\tau_0)), \quad (6)$$

where  $\mathbf{e}_\phi(\cdot)$  denotes the MLP projection of the sinusoidal embedding.

**Fidelity-Stability Trade-off.** Our key finding is that the choice of  $\tau_0$  induces a strict *fidelity-stability trade-off* that persists even after fine-tuning converges. As shown in Figure 3, early timestep (e.g.,  $\tau = 0.8$ ) biases the model toward low-frequency global structures (stable but blurry), while late timestep (e.g.,  $\tau = 0.0$ ) amplifies high-frequency details (sharp but unstable). Among the broadly similar embeddings in Figure 4, anchoring at mid-range timestep (e.g.,  $\tau = 0.5$ ) offers a low-variation conditioning region, better balancing global coherence with local sharpness (see Figure 10 for more details). We further found that completely ablating this conditioning or re-initializing significantly degrades performance, confirming  $\tau$  indexes an irreplaceable pre-trained geometric prior (Appendix §D).

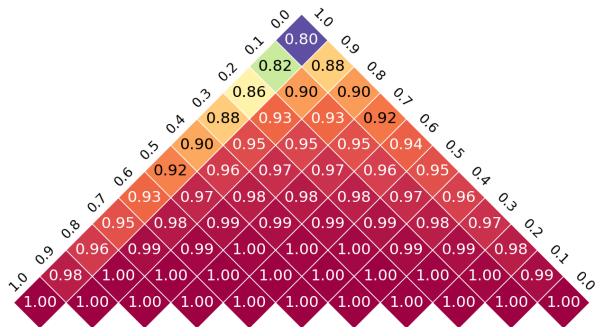


**Figure 4 Timestep embedding similarity.** Cosine similarity matrix of timestep embeddings ( $t \in [0, 1]$ , stride 0.1). While embeddings are broadly consistent, mid-range timesteps exhibit high similarity with a wider range of states.

### 4.3 Latent Manifold Rectification

While anchoring the timestep at  $\tau_0$  establishes an optimal operating regime for the backbone, training a diffusion-based deterministic regressor with point-wise objectives (e.g.,  $\mathcal{L}_2$ ) introduces a fundamental limitation, which we term **mean collapse**. Specifically, minimizing a point-wise loss to map RGB latents  $z_x$  to depth latents  $z_d$  inherently drives the predictor toward the conditional expectation  $\mathbb{E}[z_d|z_x]$  (Ma et al., 2025; Song et al., 2020a,b; Liu et al., 2022). In ambiguous or occluded regions, this regression-to-the-mean forcefully collapses multi-modal geometric hypotheses (Papayan et al., 2020; Zhu et al., 2021), washing out high-frequency structural details. Notably, this degradation is further amplified under the spatio-temporal setting: the suppressed high-frequency differentials propagate and accumulate temporally, manifesting as progressive boundary erosion and severe motion

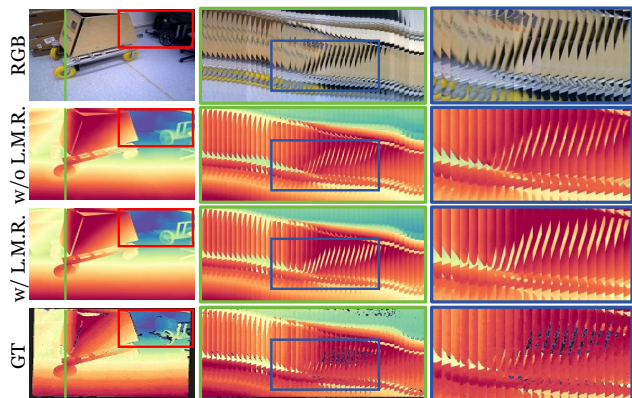


**Figure 5 LMR mitigates mean collapse.** Naive regression (2nd Row) exhibits mean collapse, losing high-frequency details. In contrast, our LMR (3rd Row) enforces differential constraints to rectify the latent manifold, recovering both sharp spatial boundaries and temporal coherence. Quantitative analyses are placed in Figure 11.

flickering, as illustrated in Figure 5.

**Differential Manifold Constraints.** To counteract this regression-induced mean collapse without introducing heavy auxiliary modules (He et al., 2025), we propose **latent manifold rectification (LMR)**, a lightweight, *parameter-free* supervision strategy that restores the local differential geometry of the prediction in the VAE latent space. LMR enforces first-order consistency between the predicted and target latents by aligning their spatial and temporal differentials. This mechanism explicitly preserves the differential statistics (gradient and flow distributions) that are typically erased by standard regression, successfully restoring sharp boundaries and coherent motion dynamics (see Figure 5).

- **Spatial Rectification (Latent Gradient).** To preserve sharp geometric discontinuities encoded within the latent space, **DVD** aligns the spatial gradient fields using finite differences  $\nabla_h, \nabla_w$ :

$$\mathcal{L}_{\text{sp}} = \frac{1}{F \cdot \Omega} \sum_{f=1}^F \sum_{\partial \in \{\nabla_h, \nabla_w\}} \|\partial \hat{z}_d^f - \partial z_d^f\|_1, \quad (7)$$

where  $\Omega$  is the spatial resolution. This explicitly penalizes low-frequency latent collapse, enforcing the recovery of fine-grained structural boundaries.

- **Temporal Rectification (Latent Flow).** Temporal artifacts correspond to mismatched dynamics in the latent depth manifold. **DVD** therefore synchronizes the predicted temporal flow with ground-truth dynamics:

$$\mathcal{L}_{\text{temp}} = \frac{1}{(F-1) \cdot \Omega} \sum_{f=2}^F \|\nabla_t \hat{z}_d^f - \nabla_t z_d^f\|_1, \quad (8)$$

where  $\nabla_t z^f = z^f - z^{f-1}$ . By constraining inter-frame differentials,  $\mathcal{L}_{\text{temp}}$  suppresses stochastic mode switching and preserves consistent motion flow.

The overall objective integrates differential rectification with global consistency:

$$\mathcal{L}_{\text{video}} = \|\hat{z}_d - z_d\|_2 + \lambda_{\text{sp}} \mathcal{L}_{\text{sp}} + \lambda_{\text{temp}} \mathcal{L}_{\text{temp}}. \quad (9)$$

Here,  $\mathcal{L}_2$  anchors the global geometry, while LMR terms act as a vital safeguard, preserving latent high-frequency structures and temporal dynamics against the smoothing effects of deterministic regression, as shown in Figure 11. Additional ablations supporting the role of LMR for deterministic regression are provided in Appendix §D.

#### 4.4 Global Affine Coherence

While LMR ensures high-fidelity spatio-temporal consistency within a given sequence, processing long videos introduces a new challenge: memory constraints necessitate sliding-window inference. In this regime, generative diffusion models inevitably suffer from *stochastic scale drift* (Hu et al., 2025; Shao et al., 2025). Their independent probabilistic sampling across windows causes non-linear geometric deformations and severe flickering, as illustrated in Figure 1. By contrast, **DVD** operates as a deterministic regressor ( $\text{Var}[\hat{z}_d | z_x] = 0$ ), fundamentally eliminating uncertain output.

**Global Affine Coherence.** Despite this deterministic stability in the latent space, naive windowed inference encounters a secondary bottleneck during pixel decoding. The VAE decoder’s context-dependent normalization inevitably induces fluctuations of depth value. Crucially, we empirically uncover a strong **global affine coherence** within our backbone. In practice, VAE decoding predominantly induces global affine variations rather than local spatial distortions, so that inter-window discrepancies can be well-approximated by a linear scale-shift transformation (Equations (10) and (11)). As validated in Figure 6, this mapping

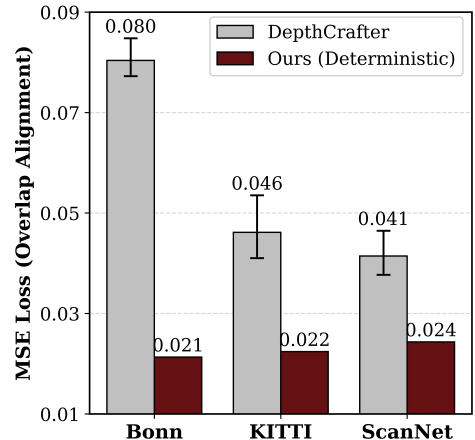


**Figure 6 Inter-window overlap consistency** (Geiger et al., 2012; Palazzolo et al., 2019; Dai et al., 2017). Unlike generative baselines with high alignment error and variance, our deterministic regression yields minimal MSE and zero variance, validating our global affine coherence that bounds inter-window discrepancies to linear transformations.

**Table 1 Zero-shot video depth estimation results.** The **best** and the second best results are highlighted.

Method	Train Frames	KITTI		ScanNet		Bonn		Sintel	
		AbsRel↓	$\delta_1$ ↑	AbsRel↓	$\delta_1$ ↑	AbsRel↓	$\delta_1$ ↑	AbsRel↓	$\delta_1$ ↑
DAv2-L (Yang et al., 2024c)	-	10.9	0.913	6.4	0.967	6.9	0.957	50.0	0.557
Marigold v1.1 (Ke et al., 2025c)	-	9.5	0.936	7.6	0.940	9.5	0.936	65.1	0.411
RollingDepth (Ke et al., 2025a)	-	9.8	0.912	5.8	0.964	5.9	0.966	43.7	0.500
ChoronDepth (Shao et al., 2025)	381K	15.2	0.775	17.1	0.818	16.8	0.901	52.8	0.504
DepthCrafter (Hu et al., 2025)	~ 30M	9.9	0.907	7.1	0.960	5.9	0.959	<b>37.1</b>	<u>0.664</u>
VDA (Chen et al., 2025d)	60M	7.2	0.963	<u>5.8</u>	<u>0.968</u>	<b>4.7</b>	<u>0.970</u>	<u>39.7</u>	0.654
<b>DVD (Ours)</b>	367K	<b>6.7</b>	<b>0.967</b>	<b>5.5</b>	<b>0.974</b>	<b>4.7</b>	<b>0.971</b>	44.5	<b>0.667</b>

**Table 2 Zero-shot long video depth estimation results.** Paradigm denotes the backbone type and inference paradigm, where "Diff.", "ViT", "D", and "G" denote Diffusion-based, ViT-based, Discriminative, and Generative, respectively.

Method	Paradigm	Bonn		ScanNet		KITTI	
		AbsRel↓	$\delta_1$ ↑	AbsRel↓	$\delta_1$ ↑	AbsRel↓	$\delta_1$ ↑
DAv2-L (Yang et al., 2024c)	Diff.+D	8.7	0.952	9.5	0.940	11.9	0.879
Marigold v1.1 (Ke et al., 2025c)	Diff.+G	11.6	0.890	12.0	0.870	24.7	0.569
RollingDepth (Ke et al., 2025a)	Diff.+G	7.2	0.966	<u>7.5</u>	0.957	11.1	0.911
ChronoDepth (Shao et al., 2025)	Diff.+G	17.3	0.859	21.2	0.715	13.0	0.846
DepthCrafter (Hu et al., 2025)	Diff.+G	8.5	0.962	11.4	0.866	12.0	0.858
VDA (Chen et al., 2025d)	ViT+D	<u>6.6</u>	<u>0.971</u>	<b>7.3</b>	<u>0.972</u>	<u>9.6</u>	<u>0.940</u>
<b>DVD (Ours)</b>	Diff.+D	<b>5.3</b>	<b>0.978</b>	<b>7.3</b>	<b>0.977</b>	<b>7.6</b>	<b>0.956</b>

aligns adjacent windows with minimal residual error. Unlike generative models suffering from unalignable stochastic distortions, our divergence is more predictable and mathematically recoverable. We further discuss the boundary conditions of this empirical observation in Appendix §E.

**Long-Video Inference.** Exploiting this well-bounded, affine-invariant property, we propose a lightweight, parameter-free *affine-alignment* strategy for sliding-window inference. Let  $\mathcal{W}_A$  and  $\mathcal{W}_B$  denote the decoded depth tensors for the preceding and current windows, respectively. **DVD** extracts the flattened depth predictions  $\mathbf{d}_A^{\text{overlap}}, \mathbf{d}_B^{\text{overlap}} \in \mathbb{R}^N$  exclusively from their  $N$  overlapping pixels. To align  $\mathcal{W}_B$  to the canonical scale of  $\mathcal{W}_A$ , **DVD** estimates a global scale  $s$  and shift  $t$  by minimizing the least-squares objective over the overlap:

$$\arg \min_{s,t} \|s\mathbf{d}_B^{\text{overlap}} + t\mathbf{1} - \mathbf{d}_A^{\text{overlap}}\|_2^2. \quad (10)$$

This yields a deterministic closed-form solution:

$$s = \frac{\text{Cov}(\mathbf{d}_A^{\text{overlap}}, \mathbf{d}_B^{\text{overlap}})}{\text{Var}(\mathbf{d}_B^{\text{overlap}})}, \quad t = \mu_A - s\mu_B, \quad (11)$$

where  $\mu_A$  and  $\mu_B$  denote the mean values of the overlapping regions. This single affine calibration is then broadcast to the *entire* current window ( $\hat{\mathcal{W}}_B = s \cdot \mathcal{W}_B + t$ ) and smoothly blends the overlapping frames via linear interpolation. This strategy enables seamless, long video inference without requiring complex feature matching, flow estimation, or recurrent temporal modules (e.g., in (Hu et al., 2025; Yang et al., 2024a; Shao et al., 2025)).

## 4.5 Image-Video Joint Training

Training exclusively on video data often compromises spatial sharpness, whereas sequential fine-tuning (image  $\rightarrow$  video) may risk catastrophic forgetting of per-frame details. To bypass this trade-off, we optimize **DVD** via an *image-video joint training* strategy. By constructing batches comprising both static images ( $F = 1$ ) and dynamic video sequences, the images act as high-frequency spatial anchors while the videos enforce temporal coherence. The unified objective is simply formulated as:

$$\mathcal{L}_{\text{joint}} = \mathcal{L}_{\text{video}} + \lambda_{\text{image}}\mathcal{L}_{\text{image}}. \quad (12)$$

This simple yet effective strategy enables **DVD** to maintain the spatial quality of diffusion priors while achieving robust temporal stability.

**Table 3 Zero-shot boundary metrics, i.e., Recall and F1.** Higher values indicate sharper boundaries and finer details.

Method	Bonn		ScanNet		KITTI	
	B-Recall $\uparrow$	B-F1 $\uparrow$	B-Recall $\uparrow$	B-F1 $\uparrow$	B-Recall $\uparrow$	B-F1 $\uparrow$
ChronoDepth (Shao et al., 2025)	0.221	0.319	0.144	0.204	0.049	<u>0.090</u>
DepthCrafter (Hu et al., 2025)	<u>0.282</u>	0.185	0.115	0.173	<u>0.082</u>	0.044
VDA (Chen et al., 2025d)	0.223	<u>0.325</u>	<u>0.147</u>	<u>0.210</u>	0.047	0.088
<b>DVD (Ours)</b>	<b>0.336</b>	<b>0.422</b>	<b>0.208</b>	<b>0.259</b>	<b>0.217</b>	<b>0.285</b>

**Table 4 Zero-shot single-image depth estimation results.**

Method	KITTI		DIODE		NYUv2	
	AbsRel $\downarrow$	$\delta_1 \uparrow$	AbsRel $\downarrow$	$\delta_1 \uparrow$	AbsRel $\downarrow$	$\delta_1 \uparrow$
ChronoDepth (Shao et al., 2025)	-	-	80.3	0.549	21.2	0.767
DepthCrafter (Hu et al., 2025)	11.0	0.877	53.3	0.592	17.1	0.868
VDA (Chen et al., 2025d)	<u>8.3</u>	<u>0.933</u>	<u>27.0</u>	<u>0.730</u>	<b>4.7</b>	<b>0.977</b>
<b>DVD (Ours)</b>	<b>8.1</b>	<b>0.944</b>	<b>23.1</b>	<b>0.738</b>	<u>5.5</u>	<u>0.969</u>

## 5 Experiments

### 5.1 Experimental Setup

**Implementation Details.** We adopt WanV2.1-1.3B (Wan et al., 2025) as our **DVD**'s backbone, fine-tuned via LoRA following (He et al., 2025). We employ a joint image-video training strategy strictly using public synthetic datasets: video clips from TartanAir (Wang et al., 2020) and Virtual KITTI (Gaidon et al., 2016) (batch size 16), alongside static images from Hypersim (Roberts et al., 2021) and Virtual KITTI (batch size 128). The entire framework converges in under 36 hours on 8 H100 GPUs, demonstrating higher training efficiency and eco-friendliness than prior arts (Chen et al., 2025d; Hu et al., 2025). More details can be found in Appendix §C.

**Evaluation.** To assess both temporal consistency and per-frame accuracy, we conduct comprehensive evaluations across two settings: ① **video datasets:** KITTI (Geiger et al., 2012), ScanNet (Dai et al., 2017), Bonn (Palazzolo et al., 2019), and Sintel (Butler et al., 2012); and ② **image datasets:** KITTI (Geiger et al., 2012), DIODE (Vasiljevic et al., 2019), and NYUv2 (Nathan Silberman and Fergus, 2012). We report standard metrics including absolute relative error (AbsRel) and threshold accuracy ( $\delta_1$ ), as well as boundary metrics like boundary F1-Score (B-F1) and boundary Recall (B-Recall) (Bochkovskii et al., 2024).

**Baselines.** We compare **DVD** with representative state-of-the-art video depth estimation methods from two paradigms: ① **generative-based:** ChronoDepth (Shao et al., 2025) and DepthCrafter (Hu et al., 2025); ② **discriminative-based:** Video Depth Anything (VDA) (Chen et al., 2025d); along with image-based Depth Anything V2 (DAv2) (Yang et al., 2024c), Marigold (Ke et al., 2025c), and RollingDepth (Ke et al., 2025a) for reference. Following standard protocols (Ke et al., 2025c; Yang et al., 2024c; Chen et al., 2025d; Hu et al., 2025), "zero-shot" denotes direct evaluation on target benchmarks without any domain-specific fine-tuning.

### 5.2 Main Results

This section provides empirical evidence of **DVD**'s effectiveness. We evaluate our approach across standard video depth benchmarks (Table 1), long-term consistency tasks (Table 2), fine-grained boundary metrics (Table 3), and single-image generalization (Table 4). Qualitative comparisons (Figure 1, 7 and 9) and rigorous efficiency & scalability analyses (Figure 8) further validate our design. Our key observations are summarized as follows:

**Obs. ① DVD achieves superior geometric fidelity and temporal coherence.** Across standard real world benchmarks (Table 1), **DVD** consistently outperforms state-of-the-art generative (*e.g.*, DepthCrafter) and discriminative (*e.g.*, VDA) baselines, achieving the lowest AbsRel on ScanNet (5.5) and KITTI (6.7). This superiority extends to long-video scenarios (Table 2), yielding a substantial margin over DepthCrafter on Bonn (5.3 *vs.* 8.5 AbsRel). Beyond global metrics, **DVD** excels at preserving fine-grained geometry. Table 3 and Figure 7

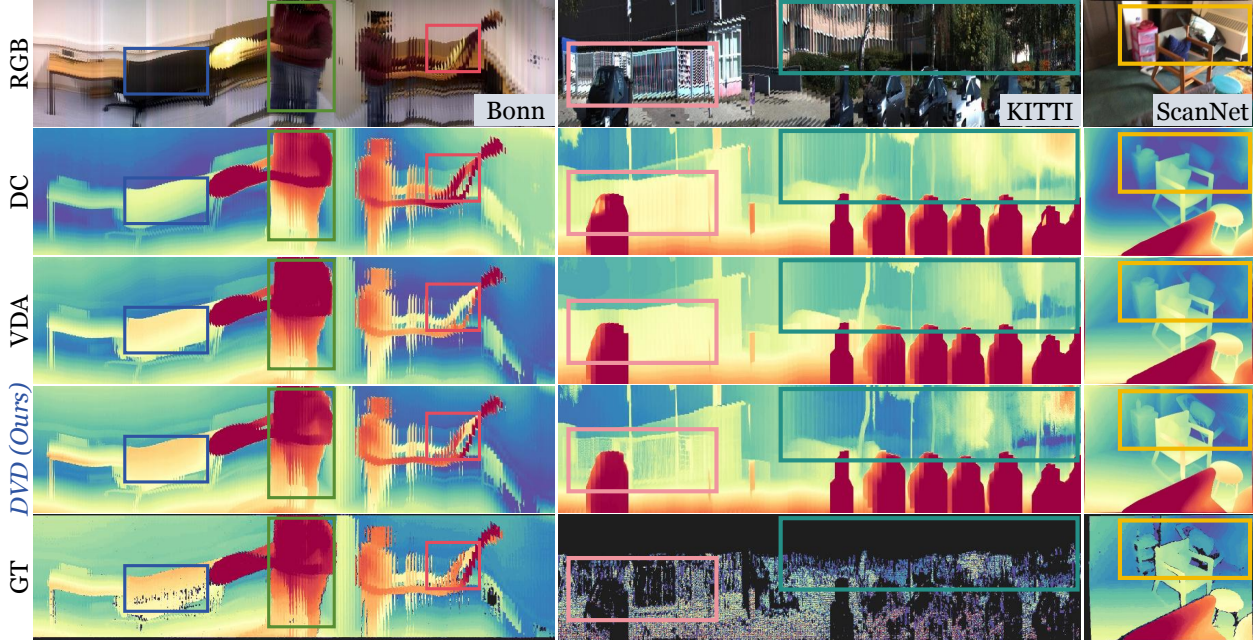


**Figure 7** Qualitative comparison on indoor and outdoor scenes. DVD consistently produces higher fidelity depth with noticeably sharper structural boundaries

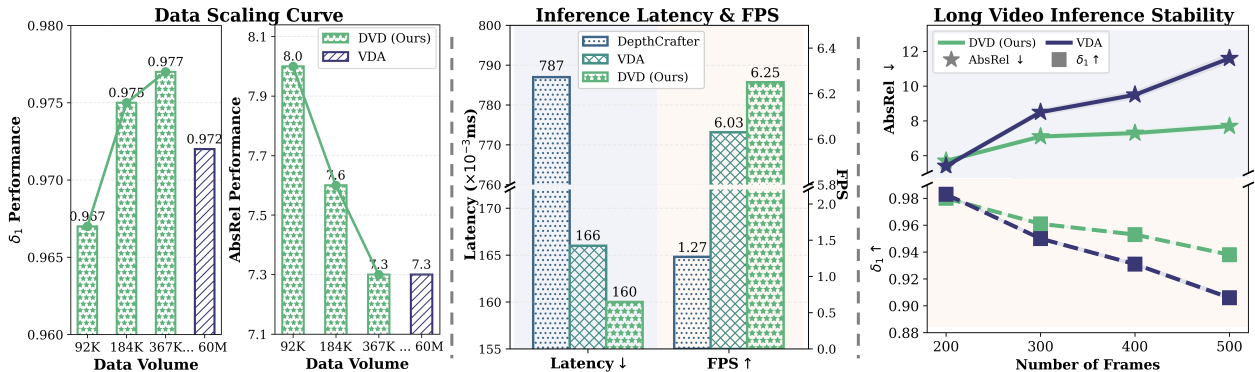


**Figure 8** (Left) Data scaling curve of long video performance on ScanNet. (Middle) Inference latency & FPS comparisons. (Right) Stability of long video inference on KITTI. These results demonstrate DVD’s remarkable data efficiency, competitive inference speed, and consistent long-video stability.

demonstrate that our latent manifold rectification successfully combats mean collapse, significantly boosting the ScanNet B-F1 score to 0.259 (compared to VDA’s 0.210). Importantly, our joint training strategy ensures this temporal robustness does not compromise spatial precision, retaining highly competitive single-image generalization, as shown in Table 4.

**Obs.Ⓜ DVD exhibits compelling data and inference efficiency.** A pivotal advantage of DVD is unlocking high-fidelity depth with minimal task-specific data and low latency. As illustrated in the scaling curves in Figure 8 (Left) and Table 1, our model trained on just 367K frames surpasses VDA, utilizing less than 1/160 of its massive dataset (60M frames). This confirms that deterministic adaptation of pre-trained world models is a vastly more data-efficient paradigm. Furthermore, as shown in the inference latency analysis in Figure 8 (Middle), DVD completely bypasses the computational bottleneck of iterative generative sampling, maintaining an inference speed comparable to efficient discriminative models like VDA while delivering superior accuracy.

**Obs.Ⓝ DVD exhibits robust scalability to long videos.** Beyond short clips, DVD maintains inherent global scale consistency across disjoint temporal windows. As visualized in the in-the-wild (Figure 1) and complex domestic (Figure 9) sequences long-video sequences, while generative methods (*e.g.*, DepthCrafter) suffer from severe scale drift and discriminative baselines (*e.g.*, VDA) persistently exhibit semantic ambiguity,

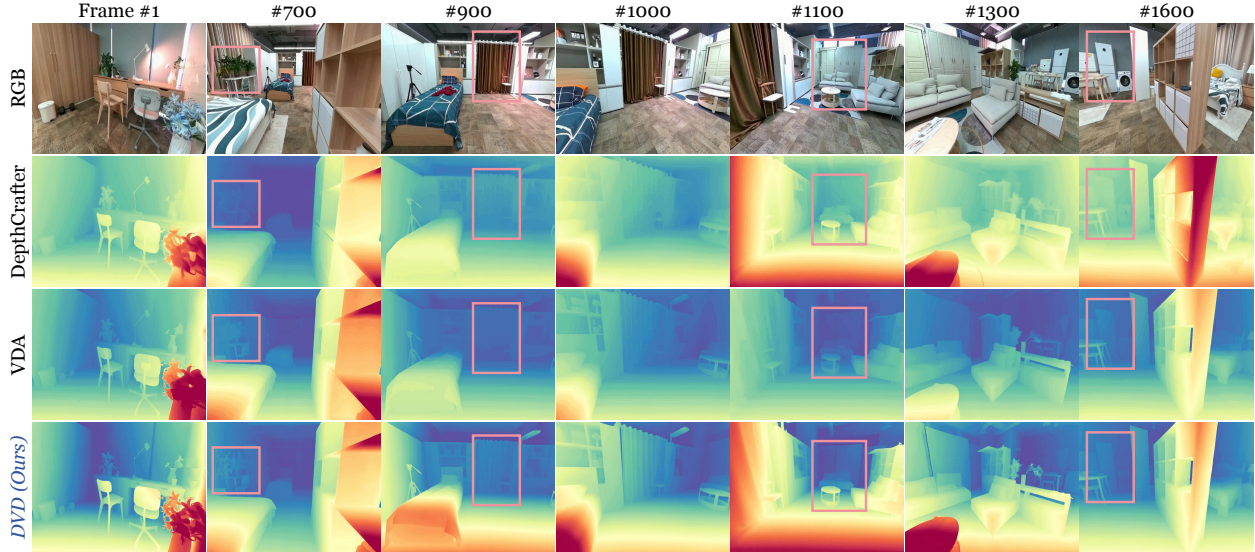


**Figure 9** Qualitative results on long-horizon indoor navigation. **DVD** leverages global affine coherence to better preserve sharp boundaries and globally coherent geometry across thousands of frames compared to prior SOTA methods.

our parameter-free affine-alignment mechanism ensures strict structural persistence and high fidelity over thousands of frames. This is quantitatively validated in Figure 8 (*Right*): as the sequence length increases, baseline methods exhibit more pronounced metric degradation, whereas **DVD** maintains more consistent stability. More qualitative analyses across diverse open-world scenes are provided in Appendix §F.

### 5.3 Framework Analysis

In this section, we analyze the core design choices of **DVD**. Unless otherwise specified, all ablation experiments are conducted on ScanNet (Dai et al., 2017). More studies are provided in Appendix §D.

**Role of Timestep Conditioning.** We first investigate the impact of the structural anchor  $\tau$  in Figure 10. The model exhibits a clear fidelity-stability trade-off, where  $\tau = 0.5$  achieves the optimal balance. Notably, comparing indoor (*Left*) and outdoor (*Right*) scenes reveals that outdoor environments are significantly more sensitive to the structural anchor, with KITTI’s AbsRel fluctuating drastically from 13.8 ( $\tau = 0.0$ ) down to 6.7 ( $\tau = 0.5$ ). Furthermore, pushing the anchor to extreme high values ( $\tau \geq 0.9$ ) triggers a severe performance collapse across both datasets, as the extreme low-frequency bias completely washes out essential geometric details. This confirms that  $\tau$  acts as a persistent structural anchor dictating the pre-trained geometric operating regime.

**Impact of Latent Manifold Rectification.** We evaluate our gradient-aware LMR modules in Figure 11 (*Left*). Adding the spatial latent gradient ( $\mathcal{L}_{sp}$ ) and temporal latent flow ( $\mathcal{L}_{temp}$ ) progressively improves both global accuracy (AbsRel drops from 8.5 to 7.3) and fine-grained boundary precision (B-F1 rises from 0.210 to 0.259). This proves that explicitly enforcing differential constraints successfully rectifies the mean collapse inherent in single-pass regression, restoring sharp structural boundaries and coherent motion. Comparisons with alternative regularizations are placed in Appendix §D.

**Deterministic Adaptation vs. Stochastic Sampling.** We compare our single-pass deterministic regression against

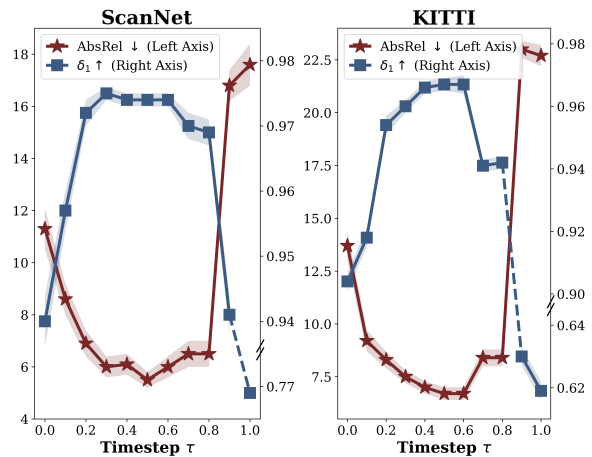


**Figure 10** Ablation of timestep  $\tau$ . The structural anchor  $\tau$  dictates a fidelity-stability trade-off. While outdoor scenes are more sensitive, both datasets achieve a balance at  $\tau = 0.5$ .

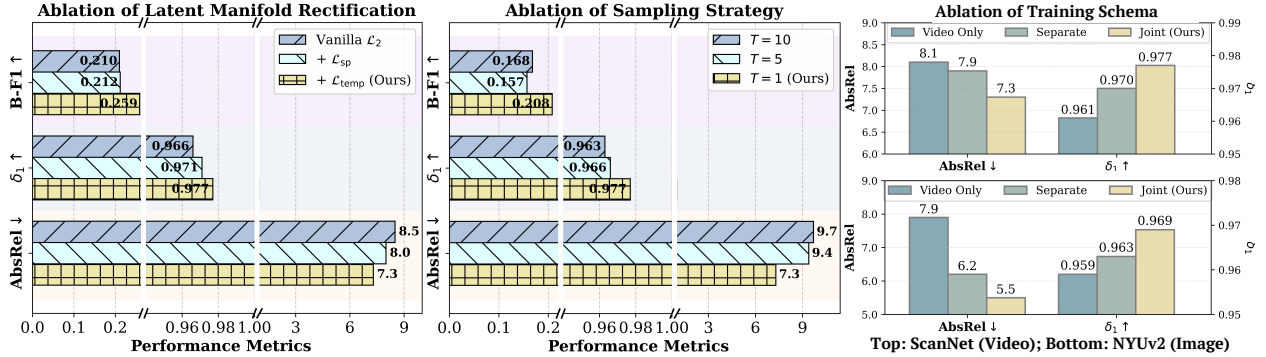


**Figure 11** (Left) Ablation of latent manifold rectification. (Middle) Ablation of the sampling strategy. (Right) Ablation of training schema. The results demonstrate that latent manifold rectification, deterministic adaptation, and joint image-video training effectively enhance geometric accuracy and structural stability.

standard multi-step sampling in Figure 11 (Middle). Our deterministic adaptation significantly outperforms generative multi-step sampling in geometric accuracy, dropping AbsRel from 9.7 ( $T = 10$ ) to 7.3 ( $T = 1$ ). This validates our core hypothesis: iterative stochastic sampling introduces aleatoric variance that manifests as geometric hallucinations, whereas our deterministic regression directly targets the conditional geometric expectation, ensuring superior structural stability.

**Effectiveness of Image-Video Joint Training.** Finally, Figure 11 (Right) analyzes our training strategy. Training exclusively on videos underfits spatial details, while separate sequential training suffers from catastrophic forgetting on single-frame tasks. Our joint strategy achieves the best performance across both domains, *i.e.*, maximizing ScanNet video accuracy ( $\delta_1 = 0.977$ ) while sharply reducing NYUv2 single-image AbsRel to 5.5. This demonstrates that images and videos offer complementary supervision: images act as high-frequency spatial anchors, while videos enforce temporal consistency.

## 6 Conclusion

In this work, we present **DVD**, the first framework to deterministically adapt pre-trained video diffusion priors for single-pass depth estimation. By bypassing stochastic sampling, **DVD** successfully resolves the ambiguity-hallucination dilemma, uniting the semantic richness of generative models with the structural stability of discriminative regressors. Our three core designs, (i) a timestep-driven structural anchor, (ii) latent manifold rectification (LMR) against spatio-temporal mean collapse, and (iii) global affine coherence for affine-alignment long-video inference, collectively establish a robust zero-shot solution. Crucially, by effectively grounding these generative priors, **DVD** achieves state-of-the-art geometric fidelity and temporal coherence while utilizing  $163\times$  less task-specific training data than leading baselines. This establishes a highly scalable and data-efficient paradigm for dynamic 3D scene understanding.

## References

- Shariq Farooq Bhat, Ibraheem Alhashim, and Peter Wonka. Adabins: Depth estimation using adaptive bins. In *Proceedings of the IEEE/CVF conference on computer vision and pattern recognition*, pages 4009–4018, 2021.
- Shariq Farooq Bhat, Reiner Birkel, Diana Wofk, Peter Wonka, and Matthias Müller. Zoedepth: Zero-shot transfer by combining relative and metric depth. *arXiv preprint arXiv:2302.12288*, 2023.
- Reiner Birkel, Diana Wofk, and Matthias Müller. Midas v3. 1—a model zoo for robust monocular relative depth estimation. *arXiv preprint arXiv:2307.14460*, 2023.
- Andreas Blattmann, Tim Dockhorn, Sumith Kulal, Daniel Mendelevitch, Maciej Kilian, Dominik Lorenz, Yam Levi, Zion English, Vikram Voleti, Adam Letts, et al. Stable video diffusion: Scaling latent video diffusion models to large datasets. *arXiv preprint arXiv:2311.15127*, 2023a.
- Andreas Blattmann, Robin Rombach, Huan Ling, Tim Dockhorn, Seung Wook Kim, Sanja Fidler, and Karsten Kreis. Align your latents: High-resolution video synthesis with latent diffusion models. In *Proceedings of the IEEE/CVF conference on computer vision and pattern recognition*, pages 22563–22575, 2023b.
- Aleksei Bochkovskii, Amaël Delaunoy, Hugo Germain, Marcel Santos, Yichao Zhou, Stephan R Richter, and Vladlen Koltun. Depth pro: Sharp monocular metric depth in less than a second. *arXiv preprint arXiv:2410.02073*, 2024.
- Tim Brooks, Bill Peebles, Connor Holmes, Will DePue, Yufei Guo, Leo Jing, David Schnurr, Joe Taylor, Troy Luhman, Eric Luhman, et al. Video generation models as world simulators. *OpenAI Blog*, 1(8):1, 2024.
- D. J. Butler, J. Wulff, G. B. Stanley, and M. J. Black. A naturalistic open source movie for optical flow evaluation. In A. Fitzgibbon et al. (Eds.), editor, *European Conf. on Computer Vision (ECCV)*, Part IV, LNCS 7577, pages 611–625. Springer-Verlag, October 2012.
- David Charatan, Sizhe Lester Li, Andrea Tagliasacchi, and Vincent Sitzmann. pixelsplat: 3d gaussian splats from image pairs for scalable generalizable 3d reconstruction. In *Proceedings of the IEEE/CVF conference on computer vision and pattern recognition*, pages 19457–19467, 2024.
- Guibin Chen, Dixuan Lin, Jiangping Yang, Chunze Lin, Junchen Zhu, Mingyuan Fan, Hao Zhang, Sheng Chen, Zheng Chen, Chengcheng Ma, et al. Skyreels-v2: Infinite-length film generative model. *arXiv preprint arXiv:2504.13074*, 2025a.
- Harold Haodong Chen, Haojian Huang, Qifeng Chen, Harry Yang, and Ser-Nam Lim. Hierarchical fine-grained preference optimization for physically plausible video generation. In *The Thirty-ninth Annual Conference on Neural Information Processing Systems*, 2025b. <https://openreview.net/forum?id=yOSRR9XGIZ>.
- Harold Haodong Chen, Disen Lan, Wen-Jie Shu, Qingyang Liu, Zihan Wang, Sirui Chen, Wenkai Cheng, Kanghao Chen, Hongfei Zhang, Zixin Zhang, et al. Tivibench: Benchmarking think-in-video reasoning for video generative models. *arXiv preprint arXiv:2511.13704*, 2025c.
- Kanghao Chen, Zixin Zhang, Guoqiang Liang, Lutao Jiang, Zeyu Wang, and Ying-Cong Chen. Event-guided consistent video enhancement with modality-adaptive diffusion pipeline. In *The Thirty-ninth Annual Conference on Neural Information Processing Systems*.
- Sili Chen, Hengkai Guo, Shengnan Zhu, Feihu Zhang, Zilong Huang, Jiashi Feng, and Bingyi Kang. Video depth anything: Consistent depth estimation for super-long videos. In *Proceedings of the Computer Vision and Pattern Recognition Conference*, pages 22831–22840, 2025d.
- Yongtao Chen, Yanbo Wang, Wentao Zhao, Guole Shen, Tianchen Deng, and Jingchuan Wang. Guided diffusion-based generation of adversarial objects for real-world monocular depth estimation attacks. *arXiv preprint arXiv:2512.24111*, 2025e.
- Jooyoung Choi, Jungbeom Lee, Chaehun Shin, Sungwon Kim, Hyunwoo Kim, and Sungroh Yoon. Perception prioritized training of diffusion models. In *Proceedings of the IEEE/CVF conference on computer vision and pattern recognition*, pages 11472–11481, 2022.
- Gene Chou, Wenqi Xian, Guandao Yang, Mohamed Abdelfattah, Bharath Hariharan, Noah Snavely, Ning Yu, and Paul Debevec. Flashdepth: Real-time streaming video depth estimation at 2k resolution. In *Proceedings of the IEEE/CVF International Conference on Computer Vision*, pages 9638–9648, 2025.

- Angela Dai, Angel X. Chang, Manolis Savva, Maciej Halber, Thomas Funkhouser, and Matthias Nießner. Scannet: Richly-annotated 3d reconstructions of indoor scenes. In *Proc. Computer Vision and Pattern Recognition (CVPR), IEEE*, 2017.
- David Eigen, Christian Puhersch, and Rob Fergus. Depth map prediction from a single image using a multi-scale deep network. *Advances in neural information processing systems*, 27, 2014.
- Xiao Fu, Wei Yin, Mu Hu, Kaixuan Wang, Yuexin Ma, Ping Tan, Shaojie Shen, Dahua Lin, and Xiaoxiao Long. Geowizard: Unleashing the diffusion priors for 3d geometry estimation from a single image. In *European Conference on Computer Vision*, pages 241–258. Springer, 2024.
- Adrien Gaidon, Qiao Wang, Yohann Cabon, and Eleonora Vig. Virtual worlds as proxy for multi-object tracking analysis. In *Proceedings of the IEEE conference on Computer Vision and Pattern Recognition*, pages 4340–4349, 2016.
- Yu Gao, Haoyuan Guo, Tuyen Hoang, Weilin Huang, Lu Jiang, Fangyuan Kong, Huixia Li, Jiashi Li, Liang Li, Xiaojie Li, et al. Seedance 1.0: Exploring the boundaries of video generation models. *arXiv preprint arXiv:2506.09113*, 2025.
- Andreas Geiger, Philip Lenz, and Raquel Urtasun. Are we ready for autonomous driving? the kitti vision benchmark suite. In *Conference on Computer Vision and Pattern Recognition (CVPR)*, 2012.
- Yuwei Guo, Ceyuan Yang, Anyi Rao, Zhengyang Liang, Yaohui Wang, Yu Qiao, Maneesh Agrawala, Dahua Lin, and Bo Dai. Animatediff: Animate your personalized text-to-image diffusion models without specific tuning. *arXiv preprint arXiv:2307.04725*, 2023.
- Tiankai Hang, Shuyang Gu, Chen Li, Jianmin Bao, Dong Chen, Han Hu, Xin Geng, and Baining Guo. Efficient diffusion training via min-snr weighting strategy. In *Proceedings of the IEEE/CVF international conference on computer vision*, pages 7441–7451, 2023.
- Tiankai Hang, Shuyang Gu, Jianmin Bao, Fangyun Wei, Dong Chen, Xin Geng, and Baining Guo. Improved noise schedule for diffusion training. In *Proceedings of the IEEE/CVF International Conference on Computer Vision*, pages 4796–4806, 2025.
- Jing He, Haodong Li, Wei Yin, Yixun Liang, Leheng Li, Kaiqiang Zhou, Hongbo Zhang, Bingbing Liu, and Ying-Cong Chen. Lotus: Diffusion-based visual foundation model for high-quality dense prediction. *arXiv preprint arXiv:2409.18124*, 2024.
- Jing He, Haodong Li, Mingzhi Sheng, and Ying-Cong Chen. Lotus-2: Advancing geometric dense prediction with powerful image generative model. *arXiv preprint arXiv:2512.01030*, 2025.
- Jonathan Ho, Tim Salimans, Alexey Gritsenko, William Chan, Mohammad Norouzi, and David J Fleet. Video diffusion models. *Advances in neural information processing systems*, 35:8633–8646, 2022.
- Wenyi Hong, Ming Ding, Wendi Zheng, Xinghan Liu, and Jie Tang. Cogvideo: Large-scale pretraining for text-to-video generation via transformers. *arXiv preprint arXiv:2205.15868*, 2022.
- Mu Hu, Wei Yin, Chi Zhang, Zhipeng Cai, Xiaoxiao Long, Hao Chen, Kaixuan Wang, Gang Yu, Chunhua Shen, and Shaojie Shen. Metric3d v2: A versatile monocular geometric foundation model for zero-shot metric depth and surface normal estimation. *IEEE Transactions on Pattern Analysis and Machine Intelligence*, 46(12):10579–10596, 2024.
- Wenbo Hu, Xiangjun Gao, Xiaoyu Li, Sijie Zhao, Xiaodong Cun, Yong Zhang, Long Quan, and Ying Shan. Depthcrafter: Generating consistent long depth sequences for open-world videos. In *Proceedings of the Computer Vision and Pattern Recognition Conference*, pages 2005–2015, 2025.
- Ziqi Huang, Yanan He, Jiashuo Yu, Fan Zhang, Chenyang Si, Yuming Jiang, Yuanhan Zhang, Tianxing Wu, Qingyang Jin, Nattapol Chanpaisit, et al. Vbench: Comprehensive benchmark suite for video generative models. In *Proceedings of the IEEE/CVF Conference on Computer Vision and Pattern Recognition*, pages 21807–21818, 2024.
- Bingxin Ke, Dominik Narnhofer, Shengyu Huang, Lei Ke, Torben Peters, Katerina Fragkiadaki, Anton Obukhov, and Konrad Schindler. Video depth without video models. In *Proceedings of the IEEE/CVF Conference on Computer Vision and Pattern Recognition (CVPR)*, 2025a.

- Bingxin Ke, Dominik Narnhofer, Shengyu Huang, Lei Ke, Torben Peters, Katerina Fragkiadaki, Anton Obukhov, and Konrad Schindler. Video depth without video models. In *Proceedings of the Computer Vision and Pattern Recognition Conference*, pages 7233–7243, 2025b.
- Bingxin Ke, Kevin Qu, Tianfu Wang, Nando Metzger, Shengyu Huang, Bo Li, Anton Obukhov, and Konrad Schindler. Marigold: Affordable adaptation of diffusion-based image generators for image analysis, 2025c.
- Bum Jun Kim, Yoshinobu Kawahara, and Sang Woo Kim. The disappearance of timestep embedding in modern time-dependent neural networks, 2024. <https://arxiv.org/abs/2405.14126>.
- Diederik Kingma, Tim Salimans, Ben Poole, and Jonathan Ho. Variational diffusion models. *Advances in neural information processing systems*, 34:21696–21707, 2021.
- Hanyang Kong, Xingyi Yang, Xiaoxu Zheng, and Xinchao Wang. Worldwarp: Propagating 3d geometry with asynchronous video diffusion. *arXiv preprint arXiv:2512.19678*, 2025.
- Weijie Kong, Qi Tian, Zijian Zhang, Rox Min, Zuozhuo Dai, Jin Zhou, Jiangfeng Xiong, Xin Li, Bo Wu, Jianwei Zhang, et al. Hunyuanvideo: A systematic framework for large video generative models. *arXiv preprint arXiv:2412.03603*, 2024.
- Hsin-Ying Lee, Hung-Yu Tseng, and Ming-Hsuan Yang. Exploiting diffusion prior for generalizable dense prediction. In *Proceedings of the IEEE/CVF Conference on Computer Vision and Pattern Recognition*, pages 7861–7871, 2024.
- Haodong Li, Chen Wang, Jiahui Lei, Kostas Daniilidis, and Lingjie Liu. Stereodiff: Stereo-diffusion synergy for video depth estimation. *arXiv preprint arXiv:2506.20756*, 2025.
- Yaron Lipman, Ricky TQ Chen, Heli Ben-Hamu, Maximilian Nickel, and Matt Le. Flow matching for generative modeling. *arXiv preprint arXiv:2210.02747*, 2022.
- Xingchao Liu, Chengyue Gong, and Qiang Liu. Flow straight and fast: Learning to generate and transfer data with rectified flow. *arXiv preprint arXiv:2209.03003*, 2022.
- Chuang Ma, Tomoyuki Obuchi, and Toshiyuki Tanaka. Neural collapse in cumulative link models for ordinal regression: An analysis with unconstrained feature model. *arXiv preprint arXiv:2506.05801*, 2025.
- Pushmeet Kohli Nathan Silberman, Derek Hoiem and Rob Fergus. Indoor segmentation and support inference from rgb-d images. In *ECCV*, 2012.
- Abby O’Neill, Abdul Rehman, Abhiram Maddukuri, Abhishek Gupta, Abhishek Padalkar, Abraham Lee, Acorn Pooley, Agrim Gupta, Ajay Mandlekar, Ajinkya Jain, et al. Open x-embodiment: Robotic learning datasets and rt-x models: Open x-embodiment collaboration 0. In *2024 IEEE International Conference on Robotics and Automation (ICRA)*, pages 6892–6903. IEEE, 2024.
- E. Palazzolo, J. Behley, P. Lottes, P. Giguère, and C. Stachniss. ReFusion: 3D Reconstruction in Dynamic Environments for RGB-D Cameras Exploiting Residuals. 2019. <https://www.ipb.uni-bonn.de/pdfs/palazzolo2019iros.pdf>.
- Vardan Papyan, XY Han, and David L Donoho. Prevalence of neural collapse during the terminal phase of deep learning training. *Proceedings of the National Academy of Sciences*, 117(40):24652–24663, 2020.
- William Peebles and Saining Xie. Scalable diffusion models with transformers. In *Proceedings of the IEEE/CVF international conference on computer vision*, pages 4195–4205, 2023.
- Duc-Hai Pham, Tung Do, Phong Nguyen, Binh-Son Hua, Khoi Nguyen, and Rang Nguyen. Sharpdepth: Sharpening metric depth predictions using diffusion distillation. In *Proceedings of the Computer Vision and Pattern Recognition Conference*, pages 17060–17069, 2025.
- Luigi Piccinelli, Yung-Hsu Yang, Christos Sakaridis, Mattia Segu, Siyuan Li, Luc Van Gool, and Fisher Yu. Unidepth: Universal monocular metric depth estimation. In *Proceedings of the IEEE/CVF Conference on Computer Vision and Pattern Recognition*, pages 10106–10116, 2024.
- Luigi Piccinelli, Thiemo Wandel, Christos Sakaridis, Wim Abbeloos, and Luc Van Gool. Video depth propagation. *arXiv preprint arXiv:2512.10725*, 2025.
- René Ranftl, Alexey Bochkovskiy, and Vladlen Koltun. Vision transformers for dense prediction. In *Proceedings of the IEEE/CVF international conference on computer vision*, pages 12179–12188, 2021.

- Mike Roberts, Jason Ramapuram, Anurag Ranjan, Atulit Kumar, Miguel Angel Bautista, Nathan Paczan, Russ Webb, and Joshua M. Susskind. Hypersim: A photorealistic synthetic dataset for holistic indoor scene understanding. In *International Conference on Computer Vision (ICCV) 2021*, 2021.
- Olaf Ronneberger, Philipp Fischer, and Thomas Brox. U-net: Convolutional networks for biomedical image segmentation. In *International Conference on Medical image computing and computer-assisted intervention*, pages 234–241. Springer, 2015.
- Team Seedance, Heyi Chen, Siyan Chen, Xin Chen, Yanfei Chen, Ying Chen, Zhuo Chen, Feng Cheng, Tianheng Cheng, Xinqi Cheng, et al. Seedance 1.5 pro: A native audio-visual joint generation foundation model. *arXiv preprint arXiv:2512.13507*, 2025.
- Jiahao Shao, Yuanbo Yang, Hongyu Zhou, Youmin Zhang, Yujun Shen, Vitor Guizilini, Yue Wang, Matteo Poggi, and Yiyi Liao. Learning temporally consistent video depth from video diffusion priors. In *Proceedings of the Computer Vision and Pattern Recognition Conference*, pages 22841–22852, 2025.
- Ivan Sobko, Hayko Riemenschneider, Markus Gross, and Christopher Schroers. Stabledpt: Temporal stable monocular video depth estimation. *arXiv preprint arXiv:2601.02793*, 2026.
- Jiaming Song, Chenlin Meng, and Stefano Ermon. Denoising diffusion implicit models. *arXiv preprint arXiv:2010.02502*, 2020a.
- Yang Song, Jascha Sohl-Dickstein, Diederik P Kingma, Abhishek Kumar, Stefano Ermon, and Ben Poole. Score-based generative modeling through stochastic differential equations. *arXiv preprint arXiv:2011.13456*, 2020b.
- Ziyang Song, Zerong Wang, Bo Li, Hao Zhang, Ruijie Zhu, Li Liu, Peng-Tao Jiang, and Tianzhu Zhang. Depthmaster: Taming diffusion models for monocular depth estimation. *arXiv preprint arXiv:2501.02576*, 2025.
- Genmo Team. Mochi 1. <https://github.com/genmoai/models>, 2024.
- Igor Vasiljevic, Nick Kolkin, Shanyi Zhang, Ruotian Luo, Haochen Wang, Falcon Z. Dai, Andrea F. Daniele, Mohammadreza Mostajabi, Steven Basart, Matthew R. Walter, and Gregory Shakhnarovich. DIODE: A Dense Indoor and Outdoor DEpth Dataset. *CoRR*, abs/1908.00463, 2019. <http://arxiv.org/abs/1908.00463>.
- Team Wan, Ang Wang, Baole Ai, Bin Wen, Chaojie Mao, Chen-Wei Xie, Di Chen, Feiwu Yu, Haiming Zhao, Jianxiao Yang, et al. Wan: Open and advanced large-scale video generative models. *arXiv preprint arXiv:2503.20314*, 2025.
- Jiuniu Wang, Hangjie Yuan, Dayou Chen, Yingya Zhang, Xiang Wang, and Shiwei Zhang. Modelscope text-to-video technical report. *arXiv preprint arXiv:2308.06571*, 2023.
- Ruicheng Wang, Sicheng Xu, Cassie Dai, Jianfeng Xiang, Yu Deng, Xin Tong, and Jiaolong Yang. Moge: Unlocking accurate monocular geometry estimation for open-domain images with optimal training supervision. In *Proceedings of the IEEE/CVF Conference on Computer Vision and Pattern Recognition*, pages 5261–5271, 2025.
- Wenshan Wang, DeLong Zhu, Xiangwei Wang, Yaoyu Hu, Yuheng Qiu, Chen Wang, Yafei Hu, Ashish Kapoor, and Sebastian Scherer. Tartanair: A dataset to push the limits of visual slam. 2020.
- Haofei Xu, Songyou Peng, Fangjinhua Wang, Hermann Blum, Daniel Barath, Andreas Geiger, and Marc Pollefeys. Depthslat: Connecting gaussian splatting and depth. In *Proceedings of the Computer Vision and Pattern Recognition Conference*, pages 16453–16463, 2025a.
- Tian-Xing Xu, Xiangjun Gao, Wenbo Hu, Xiaoyu Li, Song-Hai Zhang, and Ying Shan. Geometrycrafter: Consistent geometry estimation for open-world videos with diffusion priors. In *Proceedings of the IEEE/CVF International Conference on Computer Vision*, pages 6632–6644, 2025b.
- Honghui Yang, Di Huang, Wei Yin, Chunhua Shen, Haifeng Liu, Xiaofei He, Binbin Lin, Wanli Ouyang, and Tong He. Depth any video with scalable synthetic data. *arXiv preprint arXiv:2410.10815*, 2024a.
- Lihe Yang, Bingyi Kang, Zilong Huang, Xiaogang Xu, Jiashi Feng, and Hengshuang Zhao. Depth anything: Unleashing the power of large-scale unlabeled data. In *Proceedings of the IEEE/CVF conference on computer vision and pattern recognition*, pages 10371–10381, 2024b.
- Lihe Yang, Bingyi Kang, Zilong Huang, Zhen Zhao, Xiaogang Xu, Jiashi Feng, and Hengshuang Zhao. Depth anything v2. *Advances in Neural Information Processing Systems*, 37:21875–21911, 2024c.

- Wei Yin, Chi Zhang, Hao Chen, Zhipeng Cai, Gang Yu, Kaixuan Wang, Xiaozhi Chen, and Chunhua Shen. Metric3d: Towards zero-shot metric 3d prediction from a single image. In *Proceedings of the IEEE/CVF international conference on computer vision*, pages 9043–9053, 2023.
- Hongfei Zhang, Kanghao Chen, Zixin Zhang, Harold Haodong Chen, Yuanhuiyi Lyu, Yuqi Zhang, Shuai Yang, Kun Zhou, and Yingcong Chen. Dualcamctrl: Dual-branch diffusion model for geometry-aware camera-controlled video generation. *arXiv preprint arXiv:2511.23127*, 2025.
- Yabo Zhang, Yuxiang Wei, Dongsheng Jiang, Xiaopeng Zhang, Wangmeng Zuo, and Qi Tian. Controlvideo: Training-free controllable text-to-video generation. *arXiv preprint arXiv:2305.13077*, 2023.
- Zhihui Zhu, Tianyu Ding, Jinxin Zhou, Xiao Li, Chong You, Jeremias Sulam, and Qing Qu. A geometric analysis of neural collapse with unconstrained features. *Advances in Neural Information Processing Systems*, 34:29820–29834, 2021.

# Appendix

## A Limitations and Future Work

While **DVD** establishes a robust paradigm for video depth estimation, we acknowledge several limitations that highlight promising avenues for future research.

**Boundary Conditions of Long Videos.** In unconstrained long videos, extreme dynamics, such as prolonged occlusions, rapid illumination shifts, or erratic camera motions, can introduce local non-linear distortions that temporarily overpower our global affine assumption, leading to scale inconsistencies. Future work could explore larger temporal context windows or non-linear latent tracking to mitigate these edge cases. Detailed visual failure analyses are provided in Section §E.

**Constraints for Real-Time Deployment.** Although bypassing stochastic sampling significantly accelerates inference, **DVD** still relies on a massive video DiT backbone (*e.g.*, Wan2.1-1.3B (Wan et al., 2025)). Achieving true real-time inference (*e.g.*,  $\geq 10\text{Hz}$ ) for latency-critical on-device applications remains challenging. Promising future directions include architectural distillation and integrating efficient linear-complexity sequence models to transfer these profound generative priors into lightweight networks.

**Resolution Limits of VAE.** Operating within a highly compressed VAE latent space (*e.g.*,  $8\times$  downsampling) inherently upper-bounds the recovery of ultra-thin geometric structures at native resolutions. While our latent manifold rectification (LMR) effectively mitigates structural collapse, transitioning to higher-resolution latent spaces or fully VAE-free tokenization schemes presents a compelling direction to further push geometric fidelity.

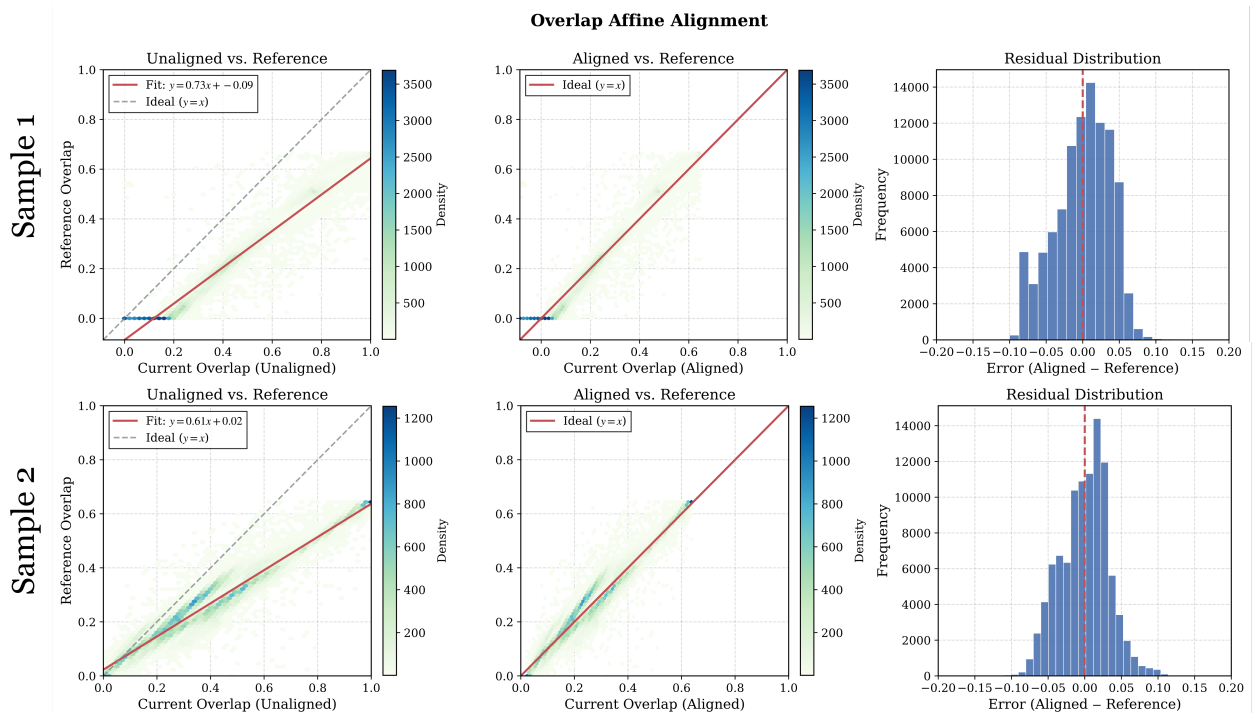


**Figure 12** Visualization of inter-window affine alignment. **(Left)** Joint pixel density distribution between the current and reference windows in the overlapping region. The strictly linear correlation (red line) confirms that the inter-window discrepancy is predominantly affine. **(Middle)** After applying our calculated affine transformation, the predictions tightly cluster along the ideal  $y = x$  diagonal. **(Right)** The histogram of pixel-wise residuals (Aligned minus Reference) exhibits a zero-mean, tightly bounded distribution with minimal variance, demonstrating the high precision of our global affine coherence strategy.

## B More Details of Global Affine Coherence

To further validate the core assumption underpinning our global affine coherence, we visualize the pixel-wise depth relationship within overlapping temporal windows here. As shown in Figure 12 (*Left*), the joint density distribution of unaligned predictions forms a strictly linear trajectory. This striking visual evidence explicitly corroborates our hypothesis: inter-window discrepancies, primarily induced by the deterministic VAE decoding, are fundamentally dominated by global scale and shift factors, rather than complex non-linear distortions. By applying our calculated affine transformation, the predictions perfectly converge onto the ideal  $y = x$  diagonal (*Middle*). Furthermore, the post-alignment residual distribution (*Right*) is strictly zero-centered with minimal variance. This demonstrates that our lightweight linear alignment strategy is effective for stitching long sequences with negligible geometric error.

## C More Implementation Details

**Training Details.** To facilitate reproducibility, we detail the architectural configurations and training hyperparameters of DVD in this section. To adapt this model for deterministic regression while strictly preserving its pre-trained world priors, we freeze the original weights and employ Low-Rank Adaptation (LoRA) exclusively on the attention blocks. The detailed settings for the VAE compression, LoRA configuration, optimization schedule, and joint-training loss weights are systematically summarized in Table 5.

**Table 5** Hyperparameter configurations for DVD.

Setting	Hyperparameter	Value
<i>Model Architecture &amp; Adaptation</i>		
<b>Backbone</b>	pre-trained model	Wan2.1-1.3B
<b>VAE</b>	spatial compression	8×
	temporal compression	4×
<b>LoRA</b>	target modules	$W_q, W_k, W_v, W_o, W_{ffn}$
	rank ( $r$ ) / alpha ( $\alpha$ )	512/512
<i>Training &amp; Inference Settings</i>		
<b>Optimization</b>	optimizer	AdamW
	base learning rate	$1 \times 10^{-4}$
	LR schedule	Constant
	hardware	8× NVIDIA H100 GPUs
<b>Data</b>	global batch size (video)	16
	global batch size (image)	128
	spatial resolution	$480 \times 640$
	window size	45
	stride (inference)	9
<i>Objective Weights</i>		
<b>Loss Weights</b>	spatial rectification ( $\lambda_{sp}$ )	0.5
	temporal rectification ( $\lambda_{temp}$ )	0.5
	image joint loss ( $\lambda_{image}$ )	1.0

**Experimental Details.** We provide more details here regarding our fine-grained evaluation protocols and inference efficiency benchmarking to ensure fair comparison and reproducibility. **❶ Video Length Partitioning.** Aggregating metrics across an entire dataset often masks the severe scale drift generative models suffer on extended sequences. To rigorously assess temporal stability, we partition the test sets by duration: *short videos* (50–200 frames) and *long videos* (> 200 frames). This explicit decoupling effectively isolates short-term geometric fidelity from long-term structural persistence. **❷ Inference Efficiency Benchmarking.** Latency and FPS are evaluated on a single NVIDIA RTX A6000 GPU under identical environments. To reflect practical deployment, we implement two streamlined optimizations: (i) merging LoRA weights into the base backbone to eliminate modular overhead, and (ii) using non-tiled VAE decoding to bypass spatial slicing bottlenecks. While our single-pass paradigm is inherently fast, integrating advanced accelerators (*e.g.*, TensorRT) remains a promising future direction for real-time edge applications.

**Table 6** Cross-backbone generalization on KITTI. We deploy **DVD** on CogVideoX-5B (Hong et al., 2022). Consistent with our default Wan2.1-1.3B backbone, the mid-range timestep ( $\tau = 0.5$ ) serves as the optimal structural anchor.

Metric	Wan2.1-1.3B	CogVideoX-5B (by $\tau$ )				
	DVD	0.1	0.3	0.5	0.7	0.9
AbsRel ↓	6.7	7.8	7.6	7.4	7.4	9.5
$\delta$ ↑	0.967	0.931	0.934	0.938	0.935	0.898

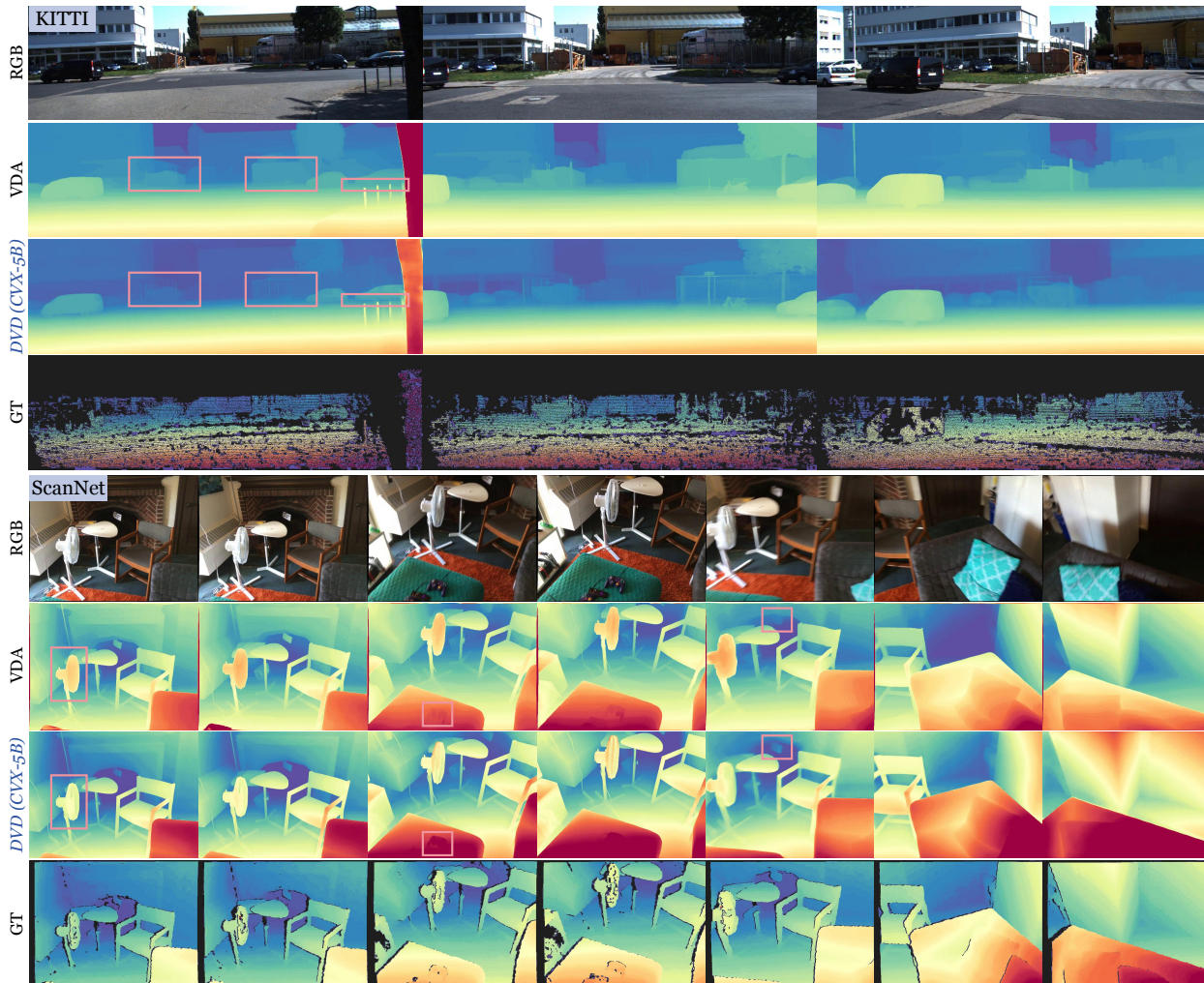


**Figure 13** Qualitative results of **DVD** on CogVideoX (Hong et al., 2022). Despite employing a different foundation architecture, our deterministic paradigm still preserves significantly sharper high-frequency details (highlighted in red boxes) compared to the leading baseline.

## D More Analysis

**Cross-Backbone Generalization.** To verify that our deterministic adaptation paradigm is universally applicable rather than specific to a single architecture, we further deploy **DVD** on CogVideoX-5B (Hong et al., 2022). As shown in Table 6, ablating the structural anchor  $\tau$  on KITTI perfectly corroborates our findings from the Wan2.1-1.3B backbone: extreme timesteps degrade geometry, whereas the mid-range value ( $\tau = 0.5$ ) provides the optimal conditioning (AbsRel 7.4,  $\delta_1$  0.938). While the CogVideoX-5B + **DVD** variant yields expectedly lower metrics than our default Wan2.1 backbone (due to differing foundation capacities and pre-training distributions), its fundamental capability for structural extraction remains profoundly robust. As visualized in Figure 13, even with a different generative backbone, **DVD** effortlessly recovers fine-grained, high-frequency geometries that are severely over-smoothed by the state-of-the-art discriminative baseline, VDA. This further confirms the broad generalizability of our zero-shot adaptation strategy across diverse generative families.

**Analysis of Pre-trained Structural Anchors.** Table 7 details the exact numerical breakdown of the fidelity-stability trade-off discussed in Figure 10. As previously established, entirely removing the structural anchor (represented as w/o  $\tau$ , which is equivalent to the  $\tau = 0.0$  boundary state) significantly degrades global metric accuracy. To further investigate whether this conditioning acts merely as a standard trainable parameter or an irreplaceable pre-trained key, we introduce a new extreme ablation: **learning  $\tau$** . In this setting, we replace the fixed sinusoidal frequency basis with a randomly initialized, fully learnable embedding of identical dimensions. As shown in Table 7, learning a new anchor from scratch triggers a catastrophic performance collapse, with AbsRel skyrocketing to 16.3 and 23.7 on ScanNet and KITTI, respectively. We attribute this to the fact that the profound structural priors within the pre-trained video DiT backbone are fundamentally entangled with its original sinusoidal frequency encodings. A newly initialized embedding fails to activate these pre-trained pathways, effectively rendering the zero-shot generative priors inaccessible. This confirms that our fixed  $\tau$  anchor natively unlocks the foundation model’s geometric capacity, and cannot be replaced by naive fine-tuning.

**Analysis of Different Regularization.** To isolate Latent Manifold Rectification (LMR)’s efficacy against mean collapse, we compare it with widely adopted regularizers in Table 8. The vanilla  $\mathcal{L}_2$  baseline yields sub-optimal accuracy (AbsRel 8.5) and structural fidelity (B-F1 0.210). Adding RGB reconstruction distracts the network toward decoding textures rather than geometry. Interestingly, existing geometric regularizers present a strict trade-off: edge-aware smoothness improves global metrics (AbsRel 7.5,  $\delta_1$  0.978) but severely over-smoothes high-frequency details (B-F1 plummets to 0.193). Conversely, multi-scale gradient matching sharpens boundaries (B-F1 0.257) but offers marginal global scale correction (AbsRel 8.2). In stark contrast, LMR breaks this dilemma. By enforcing latent differential constraints, it simultaneously minimizes AbsRel (7.3) and maximizes boundary precision (B-F1 0.259), confirming its absolute superiority for deterministic adaptations.

**Analysis of Overlap Size.** To determine the optimal balance between temporal consistency and computational efficiency, we further ablate the sliding window overlap size ( $O$ ) on KITTI (Geiger et al., 2012) here. As detailed in Table 9, an extremely small overlap ( $O = 3$ ) yields sub-optimal accuracy (AbsRel 7.9), as the limited pixel population makes the affine estimation susceptible to local dynamic outliers. Expanding the overlap region enriches the statistical basis for our Global Affine Coherence, effectively reducing inter-window discrepancies (e.g., AbsRel drops to 7.3 at  $O = 9$ ). However, further enlarging the overlap ( $O \geq 14$ ) yields diminishing geometric returns, and even saturates structural fidelity ( $\delta_1$  slightly drops at  $O = 19$ ), while incurring severe computational overhead (reaching 1.55 $\times$  relative latency). Consequently, a moderate overlap configuration provides a highly robust, jitter-free geometric transition without unnecessarily sacrificing inference efficiency.

**Analysis of LoRA Rank.** Unlike standard LoRA applications that employ low ranks for superficial style transfer, adapting a video diffusion backbone into a dense geometric regressor requires modeling highly complex mappings. Table 10 ablates the LoRA capacity on ScanNet. We observe that a moderate rank of 256 yields sub-optimal accuracy, while expanding to rank

**Table 7** Analysis of structural anchor  $\tau$ , which is evaluated on ScanNet (Left) and KITTI (Right).

Timestep	AbsRel↓	$\delta_1$ ↑	AbsRel↓	$\delta_1$ ↑
w/o $\tau$	11.3	0.940	13.7	0.904
$\tau = 0.1$	8.6	0.957	9.2	0.918
$\tau = 0.2$	6.9	0.972	8.3	0.954
$\tau = 0.3$	6.0	0.975	7.5	0.960
$\tau = 0.4$	6.1	0.974	7.0	0.966
$\tau = 0.5$	5.5	0.974	6.7	0.967
$\tau = 0.6$	6.0	0.974	6.7	0.967
$\tau = 0.7$	6.5	0.970	8.4	0.941
$\tau = 0.8$	6.5	0.969	8.4	0.942
$\tau = 0.9$	16.8	0.941	23.0	0.630
$\tau = 1.0$	17.6	0.769	22.7	0.619
<b>learning <math>\tau</math></b>	<b>16.3</b>	<b>0.811</b>	<b>23.7</b>	<b>0.699</b>

**Table 8** Analysis of regularization strategies. All variants use the same backbone, training, and inference settings.

Regularizer	AbsRel↓	$\delta_1$ ↑	B-F1↑
$\mathcal{L}_2$ only (Eq. (2))	8.5	0.966	0.210
+ RGB reconstruction	10.5	0.951	0.174
+ Edge-aware smoothness	<u>7.5</u>	<b>0.978</b>	0.193
+ Multi-scale gradient matching	8.2	0.969	<u>0.257</u>
<b>+ LMR (Ours)</b>	<b>7.3</b>	<u>0.977</u>	<b>0.259</b>

**Table 9** Analysis of overlap size on KITTI. Increasing the number of overlapping frames ( $O$ ) improves geometric accuracy but incurs diminishing returns and computational overhead (Rel. Time).

Overlap Size	AbsRel↓	$\delta_1$ ↑	Rel. Time↓
$O = 3$	7.9	0.937	1.00 $\times$
$O = 6$	7.7	0.941	1.04 $\times$
$O = 9$	7.3	0.945	1.17 $\times$
$O = 14$	7.2	0.948	1.34 $\times$
$O = 19$	7.1	0.947	1.55 $\times$

**Table 10** Analysis of LoRA ranks.

LoRA Rank	AbsRel↓	$\delta_1$ ↑
256	7.7	0.974
512	7.3	0.977
1024	7.3	0.979

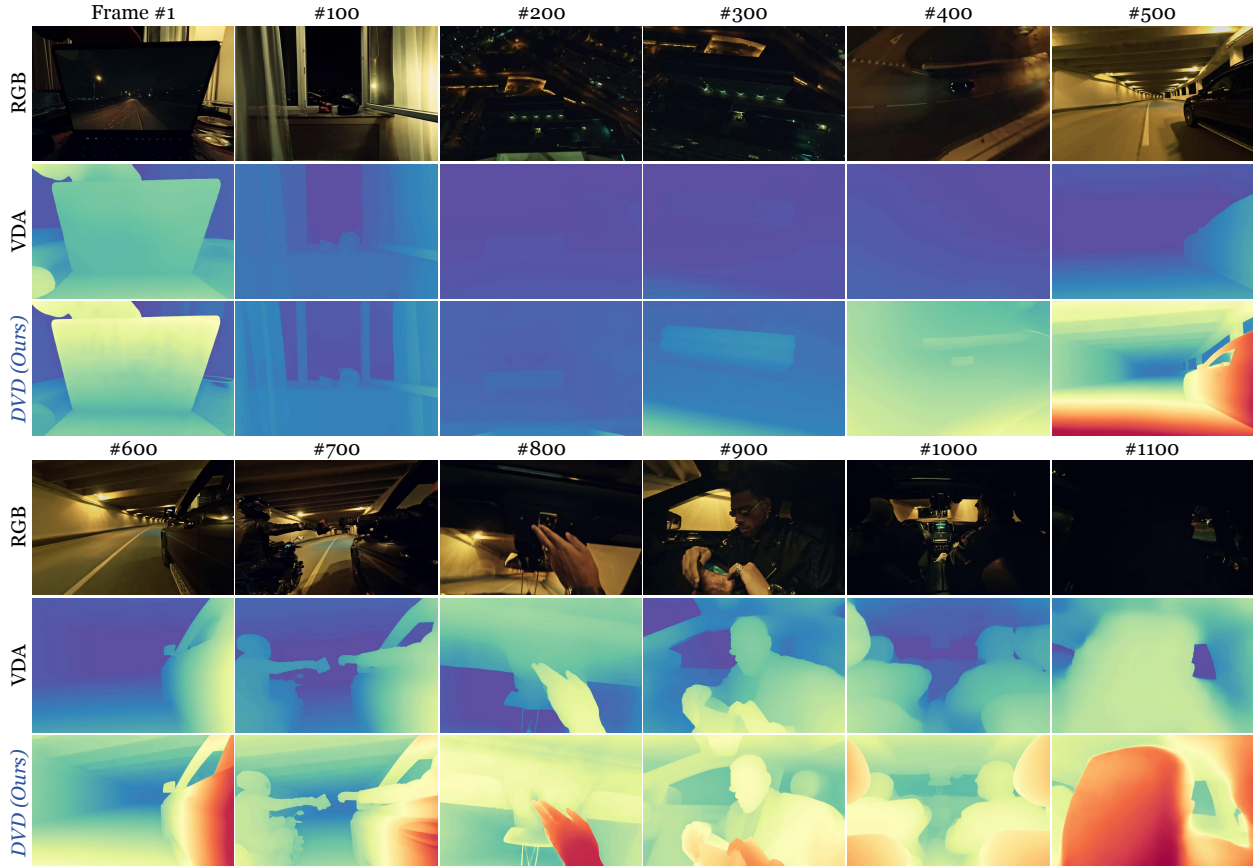


**Figure 14** Failure case analysis on 1100-frame sequence with massive scene transitions. While both **DVD** and **VDA** (Chen et al., 2025d) inevitably suffer from global scale drift across disjointed scenes (*e.g.*, contrasting the absolute depth representations between Frame #1 and #500), **DVD** consistently maintains significantly sharper local structural fidelity (*e.g.*, hands in Frames #800–#900).

512 significantly improves structural fidelity (AbsRel drops to 7.3). Further scaling to rank 1024 provides only marginal gains. Empirically, we found that extremely low ranks struggle to capture high-frequency details, whereas full parameter fine-tuning tends to overfit the limited training data and degrade the model’s pre-trained zero-shot priors. Consequently, rank 512 offers an optimal balance between geometric capacity and prior preservation.

## E Failure Case Analysis

As discussed in Section §A, the empirical affine coherence of **DVD** relies on geometric overlap between adjacent temporal windows. Consequently, the model may experience scale inconsistencies in unconstrained long-video scenarios characterized by massive ego-motion or abrupt scene transitions.

Figure 14 illustrates a highly challenging 1100-frame sequence featuring drastic environmental shifts (*e.g.*, transitioning from an indoor desk to an outdoor tunnel). When comparing distant frames with zero visual overlap (*e.g.*, Frame #1 *vs.* Frame #500), **DVD** inevitably exhibits global scale drift, struggling to anchor a unified absolute depth range across completely disjointed scenes.

Crucially, however, this limitation is an open challenge for the entire field rather than a specific flaw of our paradigm. The state-of-the-art discriminative baseline, **VDA** (Chen et al., 2025d), suffers from identical, if not more severe, temporal scale degradation under these extreme dynamics. Furthermore, even amidst global scale drift, **DVD** consistently preserves vastly superior high-frequency structural fidelity (*e.g.*, the sharp laptop screen in Frame #1 and the intricate hand geometries in Frames #800–#900) compared to the over-smoothed

predictions of VDA. This confirms that while infinite-length metric anchoring remains an unresolved problem, our deterministic generative prior still guarantees unparalleled local geometric precision.

## F Exhibition Board

To further demonstrate the robust zero-shot generalization of **DVD** across highly diverse open-world domains, this section presents an extensive exhibition of qualitative results. Our visualizations encompass a wide spectrum of scenarios, including natural landscapes, complex architecture, dynamic subjects (humans and animals), as well as out-of-domain stylized content such as animations, video games, and AI-generated videos. Detailed predictions for short video clips are provided in Figures 15, 16, and 17, while unconstrained long-video results are showcased in Figures 18, 19, and 20.

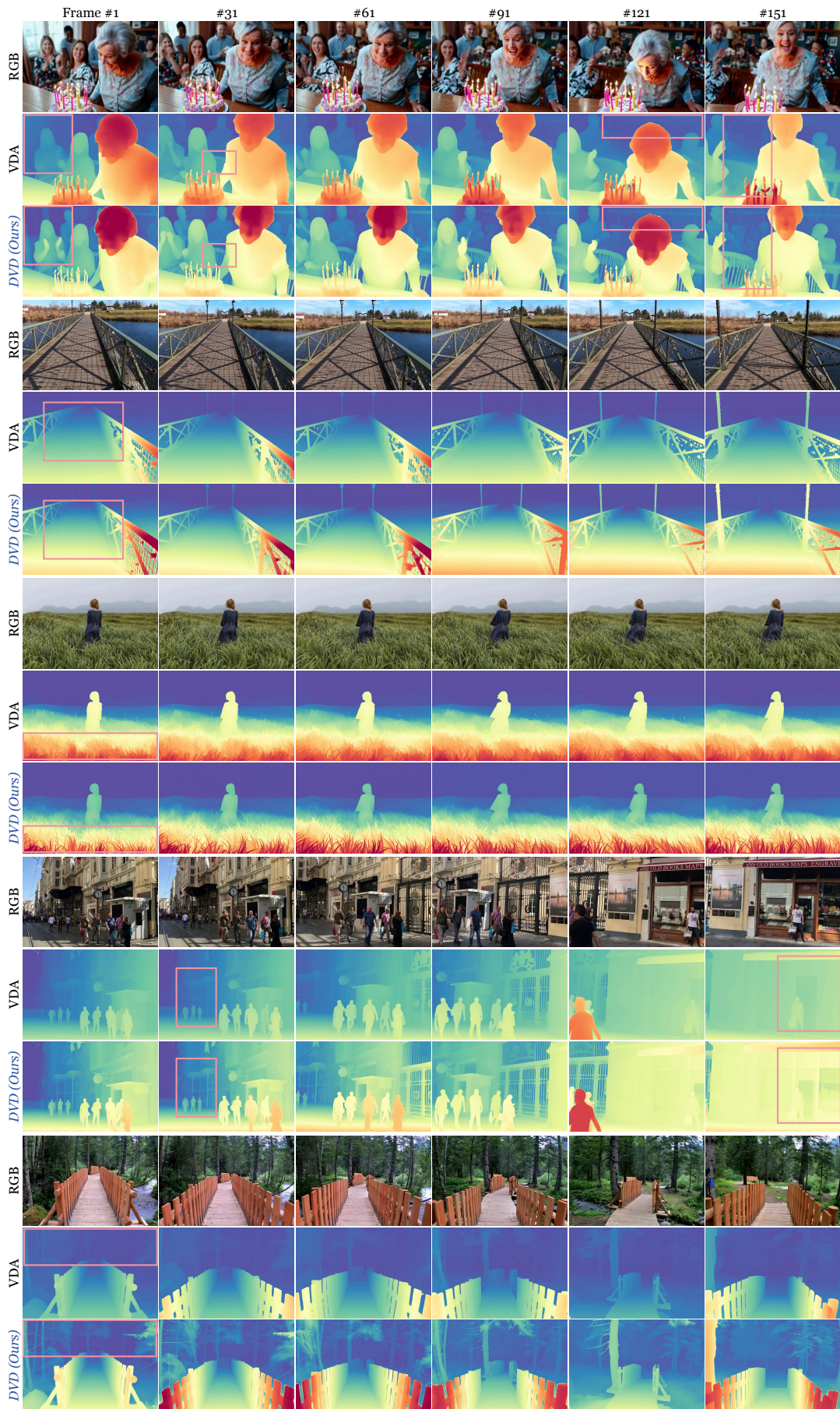


Figure 15 More results demonstrations on short videos.

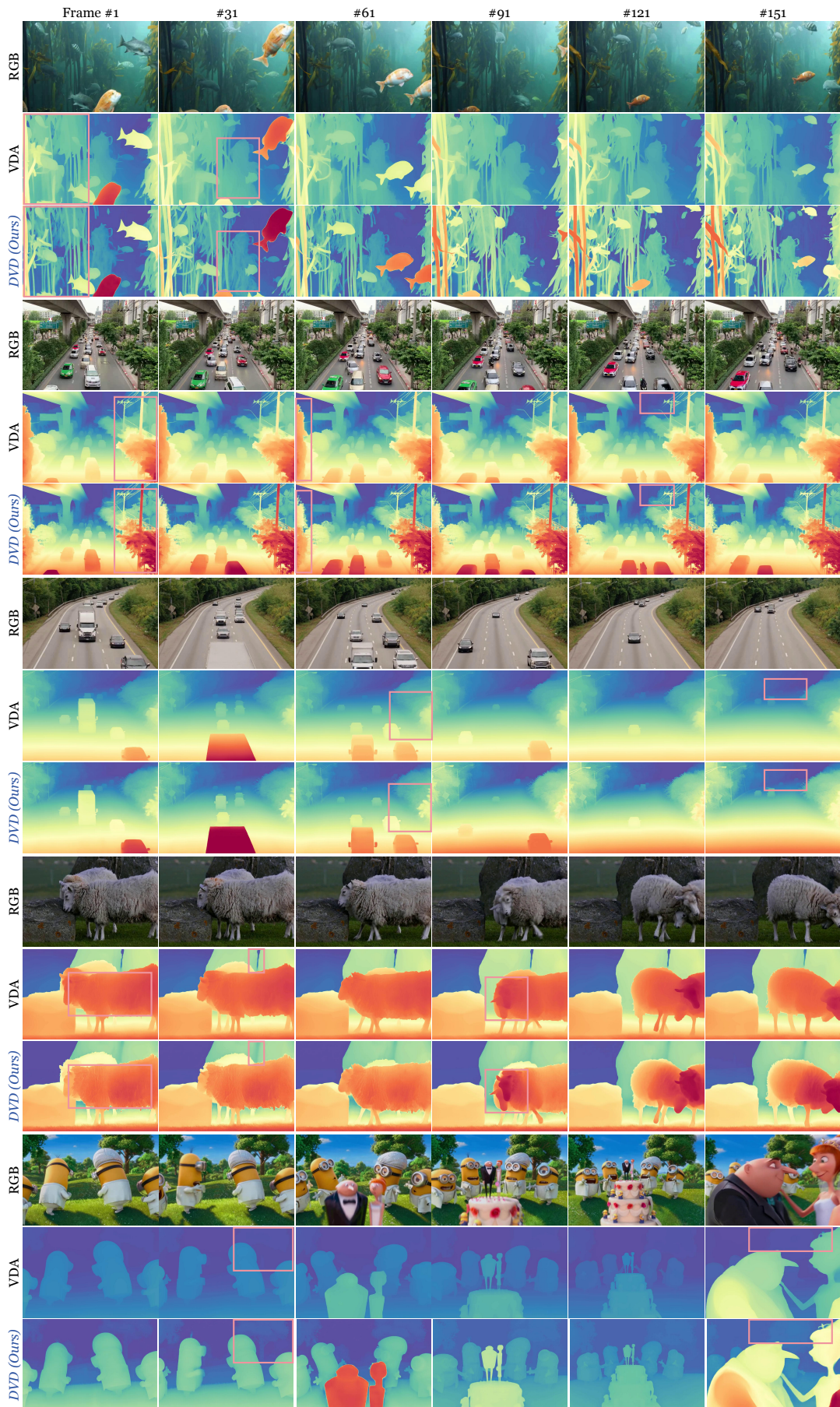


Figure 16 More results demonstrations on short videos.

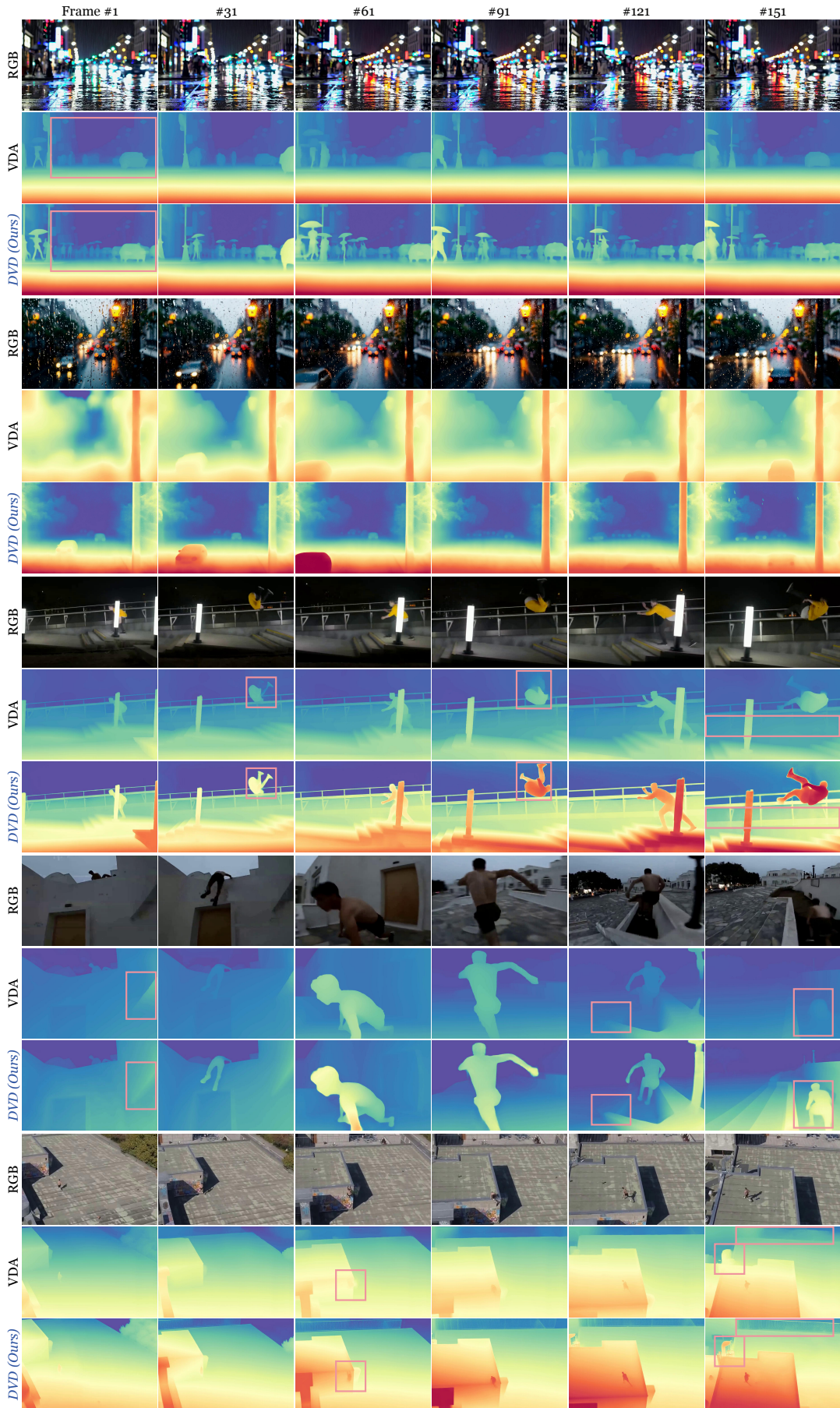


Figure 17 More results demonstrations on short videos.



**Figure 18** More results demonstrations on long videos.

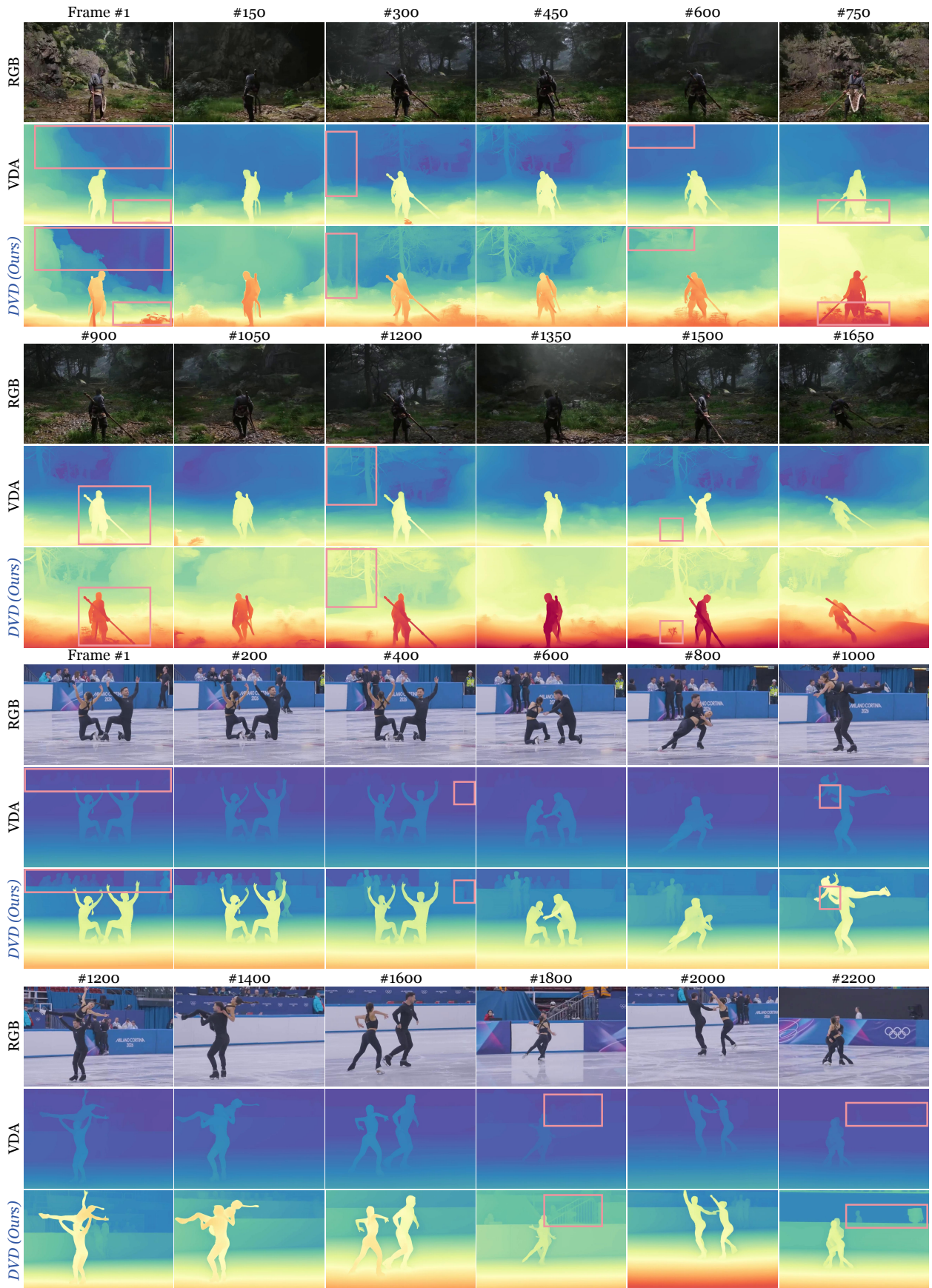


Figure 19 More results demonstrations on long videos.

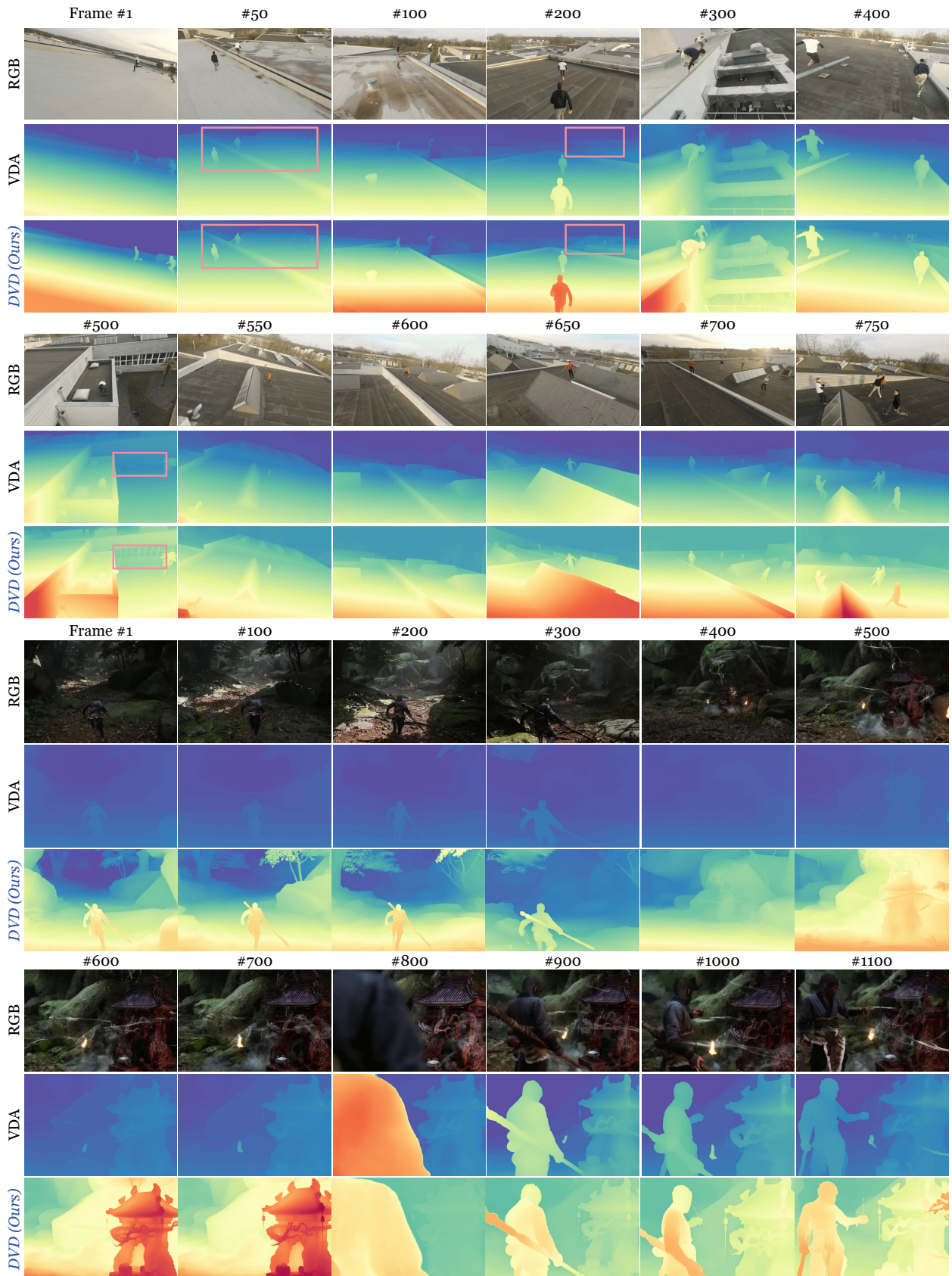


Figure 20 More results demonstrations on long videos.